Åbo Akademi

Printing and spectrometric detection of active pharmaceutical ingredients on different surfaces

Master's Thesis in Chemical Engineering, Process Chemistry

Emma Engström

Supervisor: Professor Jouko Peltonen
Co-supervisor: Anna Fogde

Physical Chemistry research group
Laboratory of Molecular Science and Engineering
Faculty of Science and Engineering
Åbo Akademi University
2021

I. ABSTRACT

Engström, Emma

Printing and spectrometric detection of active pharmaceutical ingredients on different surfaces

Master's thesis

Orion Corporation, Finland & Physical Chemistry, Laboratory of Molecular Science and Engineering, Faculty of Science and Engineering, Åbo Akademi University, 2021

Supervisors

Professor Jouko Peltonen (Åbo Akademi University)
Doctoral student Anna Fogde (Åbo Akademi University)
PhD. (Chemistry) Eero Kiljunen (Orion Corporation)
M.Sc. (Biochem.), BBA. (Acc.) Sami Pinta (Orion Corporation)

Keywords

Inkjet printing, printing of active pharmaceutical ingredients, theophylline, dosing, printing substrate, surface energy, wetting, near-infrared, infrared, Raman

Printing of pharmaceuticals is actively researched as a tailored and flexible fabricating method, towards personalized medicine. Inkjet printing is considered as a precise dosing method and in this work, theophylline is printed on eight different materials (aluminum, steel, glass, enamel, plexi, epoxy, rubber and paper) in different doses between 0.59 and 474.4 µg/cm^2 with Dimatix DMP 2830 material printer with piezoelectric, 10 pL droplet actuation. Theophylline was dissolved in a, for this printing application, optimized ink consisting of glycerol, ethanol and water in ratio 10:45:45 in concentrations between 0.06 and 11.84 mg/mL. Three different methods for adjusting the printed theophylline concentration per area were evaluated and the samples were analyzed visually and with three spectrometric methods. While near-infrared (NIR) and Raman spectroscopy showed unsatisfactory results for detecting small amounts of printed theophylline on the different surfaces, Fourier transform infrared spectroscopy (FTIR) detected printed doses as low as 2.34 µg/cm^2. Escalating printed doses of theophylline were detected both visually and by FTIR on respective surfaces. Inkjet-printed active pharmaceutical ingredients (APIs) could potentially be used as standards for cleaning validation purposes and for calibration of already established analytical instruments, as well as in the development of new promising methods for detection of small amounts of APIs on surfaces.

II. PREFACE AND ACKNOWLEDGEMENTS

This Master's thesis project was conducted in collaboration between Orion Corporation and the Physical Chemistry research group at the Laboratory of Molecular Science and Engineering. I would like to thank Orion Corporation for this opportunity and in believing in me even though the subject might have felt like a shot in the dark at first. Like a clever man named Albert Einstein once said: "If we knew what it is we were doing, it would not be called research. Would it?" I am truly satisfied with the results and I would like to thank Eero Kiljunen, Sami Pinta, Mirva Suhonen and the rest of my colleagues at Orion for all our input, support and encouragement. It has been an honor to work with you.

I would also like to thank Professor Jouko Peltonen for wise words and Anna Fogde for all her practical guidance in the laboratory as well as mental support during this process. I wish to thank the Physical Chemistry research group for welcoming me and helping me with laboratory equipment, and thanks to my fellow master's thesis workers in Gadolinia for making these months truly enjoyable.

I want to thank the members of Kemistklubben vid Åbo Akademi rf student association for keeping me hydrated and making my years of engineer studies memorable. Lastly, but certainly not least I would like to thank my life partner, Daniel, and my wonderful family for always supporting me, throughout this project and every day. I am truly thankful for having all of you in my life.

Emma Engström

Turku, May 2021

III. ABBREVIATIONS

API	Active pharmaceutical ingredient
ATR	Attenuated Total Reflection
a.u.	Arbitrary unit
CIJ	Continuous inkjet
DIM	Diiodomethane
DLS	Dynamic light scattering
DMSO	Dimethyl Sulfoxide
DoD	Drop-on-demand
Dpi	Dots per inch
DSC	Differential scanning calorimetry
DVS	Dynamic vapor sorption
EDX	Energy-dispersive X-ray spectroscopy
EG	Ethylene glycol
EHD	Electrohydrodynamic
ES	Electrostatic
EtOH	Ethanol
FDA	Food and Drug Administration (United States)
FTIR	Fourier transform infrared spectroscopy
G	Glycerol
GC	Gas Chromatography
GMP	Good manufacturing practice
HPLC	High-performance liquid chromatography
HPMC	Hydroxypropyl Methyl Cellulose
InGaAs	Indium gallium arsenide
IR	Infrared spectroscopy
MAC	Maximum allowable carryover
NDA	New Drug Application

NIR	Near infrared spectroscopy
Oh	Ohnesorge number
OPLS	Orthogonal partial least squares
PCA	Principal component analysis
PG	Propylene glycol
PIJ	Piezoelectric inkjet
Re	Reynolds number
RI	Refractive index
SFE	Surface free energy
SHG	Second harmonic generation
SNV	Standard normalized variate
TGA	Thermogravimetric analysis
TIJ	Thermal inkjet
TOF SIMS	Time-of-flight secondary ion mass spectrometry
UV–vis	Ultraviolet–visible spectroscopy
W	Water (Purified water)
We	Weber number
WHO	World Health Organization
XRD	X-Ray diffraction

IV. VARIABLES AND PARAMETERS

γ^{acid}	Acid component of surface tension
γ^{base}	Base component of surface tension
d	Characteristic length, e.g. the diameter of a nozzle jet or droplet
Θ_γ	Contact angle / Young contact angle
ρ	Density
γ^d	Dispersive component of surface tension
γ^p	Polar component of surface tension
t	Running time
γ_{LS}	Surface energy liquid-solid
γ_{LV}	Surface energy liquid-vapor
γ_{SV}	Surface energy solid-vapor
σ	Surface tension
γ^{tot}	Total surface energy
V	Velocity
η	Viscosity
k	Viscosity constant

V. TABLE OF CONTENTS

1 INTRODUCTION

1.1 Background

All humans are not biologically the same and a need for personalized medicine and a mindset of "one dose does not necessarily fit all" have emerged during the last decades. This mindset especially applies for some specialized medicine (such as breast cancer treatment), where sex, age, race, weight and biology of the patient, play an important role in uptake of the medication and the bioactivity in body. Printing of pharmaceuticals has been proven to be an additive manufacturing method in aspect to customization and flexible dosing opportunities. Additive manufacturing has already been used in e.g. the automobile industry to 3D-print spare parts according to the costumer's specific need, rather than being limited to traditional fabrication. During the last decade, both 2D and 3D printing technologies have been proven promising for several medical applications. Benefits include low production cost, negligible variability (unit-to-unit), and of course high flexibility for customization, both for therapeutical and biomedical applications such as organs and artificial tissues. In 2015, the first printed drug, SPRITAM® (levetiracetam) by Aprecia Pharmaceuticals Company, entered the market. The technology uses a 2D inkjet printing technique to build a 3D structure layer by layer [1]. [2]

The most research that have been done on printing of APIs, are products intended to be consumed either by injection, inhalation or orally. The printing substrates (substrate is the word generally used to describe the material, onto which an ink is printed), are usually porous; powders or liquid- or orally dispersible films. Another, less studied point of view is how printing of pharmaceuticals can be utilized in other areas in the pharmaceutical industry. The focus of this thesis was to explore printing of small amounts (µg) APIs of different materials used in dug production facilities and to investigate the lowest detectable amount of printed API on different surfaces. Printing could potentially be used for prototyping of drug residuals in production vessels and pipelines, to exhibit precise drug amounts as standards for cleaning validation purposes. The printing substrates and associated challenges (e.g. coatings for better ink absorption, bioavailability and toxicity) in this work, differ essentially from previously done studies. Regardless of application, the underlying barriers for printing of pharmaceuticals can still be considered remaining. These can be categorized as following: 1) formulation of ink 2) ink delivery equipment 3) drop formation 4) impact, phase change and stability 5) quality of printed result and characterization. [3]

1.2 Project background

Orion Corporation (Orion Oyj) is a globally operating, Finnish pharmaceutical company established in 1917, with a net sale of EUR 1,078 million (2020) and has an extensive portfolio with hundreds of products, both human and veterinary pharmaceuticals. The products include healthcare prescription drugs and other products for illness treatment and prevention. Orion's product selection can be divided into four categories: trademarked drugs developed by Orion, generic drugs, licensed drugs patented by other pharmaceutical companies, self-care products such as basic ointments, vitamins and non-prescription medicines. These include tablets, gels, ointments, injections, inhalation products, API production (Fermion Oy) with various different production lines. [4]

Orion works under pharmaceutical, good manufacturing practice (GMP) and is regulated by authorities (both national and international) to guarantee drug quality, purity, safety and potency for consumers. These include precise standard operating procedures, quality management systems and cleaning validations [5]. Cleaning validation is extremely important and inevitable for drug production to exclude cross-contamination (detergent, microbial, or API). Visual inspection, rinse sampling and surface sampling are the three prominent standard procedures to assure cleanness in the pharmaceutical industry. Surface sampling is preferably made with swabbing or wiping and measured with off-line high-performance liquid chromatography (HPLC), which can be both costly and time consuming with respect to sample preparation and analysis time [6]. To avoid adding production delays and still assure GMP cleanness standard, in-, on-, or at-line methods with direct or non-contact sampling could be preferred for cleaning validation. Spectrometric analytical methods are known for being rapid, accurate and have low/no sampling cost and handheld devices could be a new method of operation. The limiting factors are the detection limit and calibration of the instrument for pharmaceutical validation. [6]

With an accurate dosing method, it would be possible to model standards for drug residue limits and maximum allowable carryovers (MAC). Printed API series could be used for calibration of both currently used analytical instruments and new promising methods for detection of small amounts of APIs on surfaces. Inkjet is a non-contact printing method with controlled deposition of small droplets (pL) onto a substrate, according to a preset digital design pattern. The focus of this thesis work was an investigation in inkjet printing of small amounts of API on different substrates and to analyze the prints with spectrometric methods to scope the rough detection limits in different methods and wavelengths.

1.3 Objectives

The focus of the thesis work was primarily to apply small amounts of theophylline on different surfaces by using piezoelectric inkjet printing. The aims of the work were to:

1. Prepare API (theophylline)-containing inks with the suitable printing properties
2. Optimize the printing conditions
3. Print the inks onto different materials (substrates) used in drug production facilities
4. Print series of different doses of API onto the substrates
5. Compare the prints visually and by three spectrometric methods (NIR, FTIR, Raman)

2 THEORY

2.1 Inkjet printing

2.1.1 Inkjet printing in a historical perspective

The first inkjet printer was a medical strip chart recorder produced by Siemens in 1950. During 1970-1980, inkjet printing was commercially developed for labelling and marking products with dates, bulk numbers, and bar codes. The printers used continuous inkjet (CIJ) technology, but in the mid 1980´s, a technology with much higher printing resolution was developed. The new method used drop-on-demand (DoD) technology and was a much more accurate and cost-effective way of printing. [7] [8]

From there on, printing as technology has blossomed and at the beginning of 2000, inkjet printing was one of the world's most actively patented technologies with close to four thousand patents [7]. Inkjet printing has evolved from a marking and labelling technique to a desktop, consumer and home-office printing technique and today, wide range of industries use inkjet printing. Some examples are 3D rapid prototyping, conductive patterns of costly materials, automotive coatings, ceramics and plastic part decorations [7].

Inkjet printing is already established in pharmaceutical industry for packaging and distribution activities such as serialization and traceability. While pharmaceutical materials are not printed in these applications, the technology is familiar for most pharmaceutical companies, which enables a rapid uptake in possible manufacturing context with in-house expertise. The pharmaceutical field has countless of possibilities for inkjet printing, many of which are already under research. Inkjet printing has potential in fast fabrication of a discovered drug, in advanced drug delivery applications and for manufacturing of personalized medicine. Compared to other prototyping methods, inkjet is considered user friendly with relatively straightforward computer graphical design possibilities. This allows for rapid prototyping of e.g. biomaterials for biological applications. [3] [7]

2.1.2 Inkjet printing technologies

Today, there is a wide range of different methods of printing, both conventional and digital. Conventional printing uses a designed printing plate to physically print the pattern and the methods are therefore called impact printing. How the pattern is transferred is what mainly

differentiates the conventional methods from each other. Digital printing methods, in contrast, use digital designs prepared by a software to produce patterns or 3D objects. The available technologies can be divided into inkjet-, laser- and extrusion-based printing technologies [9] [10]. Some also consider electrospray technology as a category of its own [8].

This thesis focuses on inkjet printing which is mainly divided into two main methods and several sub-methods. The main methods are CIJ and DoD printing (see Figure 1). CIJ is usually more robust and is used industrially for date-mark and code printing, while DoD printers dominate the home printer market [3]. The CIJ printing method uses a continuous stream of liquid ink that naturally breaks down into a stream of smaller droplets from which those to be printed are selected by an induced electrical field and printed onto the substrate [11]. The excess ink droplets can be collected and recirculated. DoD, in turn, makes individual droplets on an impulse [12]. The DoD methods can be divided into different categories according to how the impulse is initiated, by a thermal, piezoelectric, electrostatic or electro-hydrodynamic element (see Figure 1) [8] [9]. The focus of the thesis is on piezoelectric inkjet (PIJ) printing technology, but all inkjet technologies are shortly described.

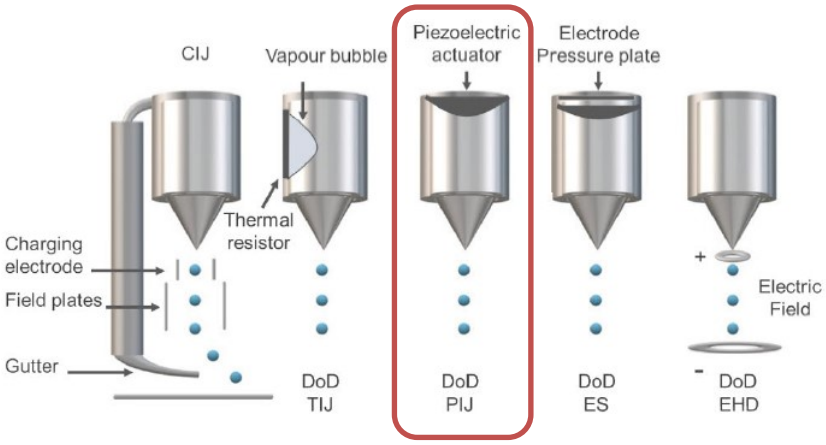

Figure 1. Overview of Continuous (CIJ) and Drop on Demand (DoD) inkjet printing technologies: Thermal (TIJ), Piezoelectric (PIJ), Electrostatic (ES) and Electrohydrodynamic (EHD) inkjet printing. The focus of this work is on PIJ actuation. (Modified from H. Wikström [9])

Thermal inkjet (TIJ) actuation utilizes the heat expansion and evaporation of the printing fluid to form a droplet. This happens by rapid heating of a small part of a chamber containing the ink, which causes the ink above the heater to vaporize and push a droplet of ink through the nozzle. While the advantages of thermal inkjet printing are compact and low-cost devices, it

is strongly limited by the ink fluids. The ink needs to both withstand high local temperatures (200-400 °C) and have the right vaporization properties. [10] [13]

TIJ was a popular technology in consumer desktop printers, but piezoelectric DoD droplet generation has fewer design constrains and has become the dominating technique in home and office printers. It is also the main technique used in printheads for industrial applications such as digital fabrication.

PIJ actuation utilizes the distortion of a piezoelectric material when under an electrical field. By creating an electric impulse, the piezoelectric wall of the ink chamber changes shape or size, which creates a pressure pulse in the fluid, forcing an ink droplet from the nozzle orifice. An often-used material for piezoelectric actuation is lead zirconate titanate, which is a ceramic material with a strong piezoelectric effect. The piezoelectric effect is described as the material's ability to cause an electric field as a response of mechanical strain, or more importantly, change shape under presence of an electric field. The piezoelectric effect is depending on the poling effect of dipoles in a material that expands or contracts according to in which direction the electric field is applied. Several actuation mechanism techniques have been developed utilizing these effects. The push-mode actuator directly uses the expansion-contraction effect to physically make the thin sheet of a piezoelectric material push a membrane which modifies the volume of the ink container and pushes ink through the nozzle [14]. Waveform is a term used for describing how a fluid is jetted (voltage ramp) and the firing voltage and amplitude is usually tuned according to the rheology of the ink [15]. While piezoelectric actuation normally is more expensive than thermal actuation, piezoelectric actuation can print a wide range of different fluids, which gives a wider freedom for ink formulation development. [7] [8]

Electrostatic (ES) inkjet actuation works similarly to the piezoelectric technique: a pressure plate in the ink chamber moves by a voltage pulse formed between an electrode and the plate [16]. This will reduce the space in the chamber and physically eject a droplet. Electrohydrodynamic (EHD) inkjet actuation works by an induced electric field between the substrate and the nozzle, which forms a high voltage and a conductive ink droplet is ejected. While the technique implementation is high-cost and only niched for some specific inks, electrohydrodynamic printing is able to print extremely small droplets (0.2-2 µL) of high viscous inks and the drop size is adjustable during printing since it is a function of the induced electric field. [17] [18]

The four main types of inkjet inks are water-based, solvent-based, phase-changing (hot melts) and UV-curable ink. Hybrid ink types of these also exist. Other inks, such as oil-based and liquid toner inks, are available but not as common. If the ink is intended to be ejected by an electrical field (CIJ, EHD), the ink must obviously contain a charge control agent for the printing technique to work. The conductivity of the ink is crucial, and agents need to be soluble in the ink. Normally, electrolytes or ionic surfactants are used as charge agents. This thesis, however, focuses on solvent-water based inks. [7]

Inkjet-printed drop diameters are typically 10-100 µm, with a drop volume of 0.5-500 pL. The most used printing technologies, TIJ and PIJ, typically have nozzle orifice diameters of 10-50 µm, and drop volumes of 1-70 pL [3] [8] [12]. Most DoD printheads have several printing nozzles (up to several hundred nozzles), arranged in a linear row or in a two-dimensional matrix. This streamlines and speeds up the printing process. The printhead (or heads) is normally fixed in a movable framework over the substrate, which allows printing larger areas than the dimension of the printhead. Commonly, the printhead moves along one axis and the substrate in perpendicular direction, step by step. By using a moving printhead, the printing resolution can be increased by overprinting (see Chapter 2.1.4). The printhead (or heads) unit is usually removable and replaceable in a printer and normally has some fine-tune alignment options (mechanical or electronic) for flexible printing options. [7]

2.1.3 Ink printing process, drop behavior and evaporation on the substrate

A PIJ drop actuation begins with an application of a voltage change (a positive pressure pulse) which makes the piezoelectric material ink chamber change shape or size, which results in extrusion of ink from the nozzle. The jet of ink then necks down and breaks off from the nozzle. Typically, after the break-off, the jet includes a bigger head containing most of the ink and a filament extending behind the head. The surface tension of the ink forces the jet into pulling all the liquid into a fully spherical droplet, as it moves downwards towards the substrate (see Figure 2) [19] [20]. The piezoelectric meniscus retracts, and the ink chamber refills by either capillary (surface driven) forces, Bernoulli underpressure effect or due to damping oscillations caused by releasing of the droplet. Time for a whole cycle is between 5-250 µs and droplet volumes are set according to ink cartridge. A PIJ printer is normally capable of printing 10 000-30 000 droplets per second. [7] [8]

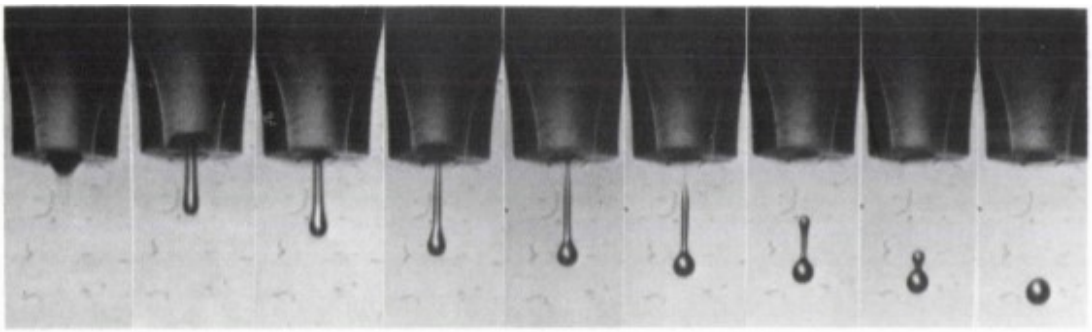

Figure 2. A series of photos showing the successive stages of an inkjet droplet formation. [21]

Satellite droplets are additional droplets that may be produced during inkjet printing. These additional droplets are smaller than the intended droplet and follow it like a tail of pearls. Satellite droplets are a result of a collapse of surface tension and filament forming one or several droplets instead of condensing into one united droplet. This is a characteristic trait for when conditions for ink properties and print actuation (waveform) are not fully met and can cause a number of problems, such as printing quality defects and equipment malfunction due to contamination. Since the satellite droplets are smaller than the main droplet, they are not influenced by gravitational forces in the same way which means that the satellite droplet may not necessarily land on the intended spot on the substrate or end up in an undesired location in the printer construction. In practical printing applications, the presence of satellite droplets can be tolerated to some extent, especially if the satellite droplet unites with the original droplet on the substrate. [3] [7] [8]

Satellite droplets can be reduced or eliminated with nozzle design, the waveform settings for the transducer drive and/or by tuning the amplitude of the initial droplet impulse [8] [22]. These are often ink-specific settings according to ink's specific properties and its behavior when fired from the nozzle. Some PIJ printers also eject subtle vibrations and by that help the droplet to break off cleanly [23].

In a printing process, a droplet is fired from the nozzle and flies towards the substrate with a velocity depending on the firing voltage and gravitational forces according to the mass of the droplet (see Figure 3). On its way towards the substrate, the droplet is possibly losing some mass due to solvent evaporation, which might affect the speed of the droplet [24]. When the droplet falls as a sphere, the initial energy state can be divided into two components: kinetic energy and surface energy [25]. When a droplet with a specific volume and certain speed hits the surface, it changes shape, starts spreading and wets the surface according to the

properties of the ink and the substrate (see Chapter 2.2.3) [26]. On a non-absorbing substrate, the kinetic energy is transferred into excess surface energy and a small amount of heat during oscillatory motion of the fluid when retracting (viscous dissipation) until an equilibrium is attained [8].

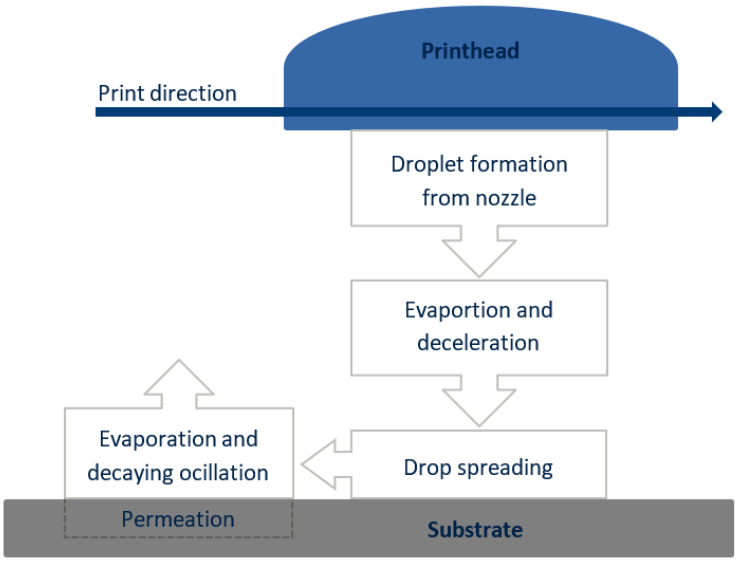

Figure 3. A schematic overview of the inkjet printing process. In case of an absorbing substrate, substrate permeation will take place. (Recreated from Hutchings *et al.* [8])

During solvent evaporation, the contact line pinning occurs in two stages: 1) the droplet-substrate contact area remains the same while the contact angle is reduced 2) contact line reacts and the contact area decreases [27]. During solvent evaporation, the fluid mass loss is proportional to the droplets spreading on the surface and liquid-vapor interface. A general rule of thumb is that a droplet with smaller initial contact angle has a higher evaporation rate. In case of an absorbing substrate, spreading, permeation and evaporation occur parallelly, partly in and partly on the substrate [28]. Drying is also limited to the thermal properties of the substrate. One way of speeding up the drying process is by heating the substrate during printing, but this might also affect the viscosity of the ink and, furthermore, it's spreading on the substrate. [7] [8]

In most cases, the ink contains solid particles or dissolved substances and these will discharge from the solution due to the solubility limit and as the solvent carrier evaporates, the contact line decreases and particles are left and form a spot on the surface [29]. A so-called coffee

staining effect can occur where the solid material only forms a ring around the original contact line and the center is free of deposit when the solvent has evaporated. This deceases the print quality. [30]

2.1.4 Print resolution

Printing resolution is a term for describing the closest spacing of individually printed spots of ink, conventionally described as dots per inch (dpi). Horizontal and perpendicular dpi may differ from each other based on print head direction. Dpi correlates to the space between printed droplets, drop spacing. The resolution depends on printed droplet's size, nozzle spacing, printhead, substrate and the movement of these. [8]

Grey scale printing is an excellent example of innovative printing where dpi plays an essential role in the printing technique [8]. Normally, one nozzle prints one size droplet and by adjusting the closeness of printed droplets or by printing several overlapping layers, one single ink can behave as several different.

Since most manufactured printheads have numerous nozzles, often in several rows, the inter-nozzle row gap might be larger than the required printing resolution, perpendicular to the printing direction. This challenge can be overcome by:

- Overprinting the same area. By moving the printhead several times over the same area, it is possible to fill in the empty gap and attain a higher dpi.
- Adjusting the angle of the printhead, printhead motion and droplet ejection timing, droplets can be printed closer together in perpendicular direction to print direction.
- Using several printheads for the same printing area. The heads can be positioned so that they can print interleave spots and achieve a higher printing resolution. [8]

Dpi is limited by the ink's wettability on the substrate. Depending on the size of the printed ink droplets and the drop spacing, the ink droplets´ absorption or spreading on the substrate might result in overlapping or merging. The physical and chemical interaction between the ink and the substrate are essential for printing and the properties are tunable with pre- or post-treatment such as substrate coating, printing conditions and drying or/and curing conditions. [8]

2.1.5 Inkjet printing of Pharmaceuticals

Most research of inkjet printing of pharmaceuticals has been done on DoD technology rather than CIJ. The small volume of liquid required for DoD printing is an advantage. On the other hand, recirculation of the CIJ-ink might be a risk for contamination. DoD printheads usually have multiple nozzles (up to 1000), but some special printheads only have a single nozzle. [3]

A wide range of different materials, including nanomaterials, cells and colloids have previously, successfully been inkjet-printed and inks containing particles (e.g. pigmented inks), have already been industrially printed for decades. Firstly, solid pharmaceuticals are limited by concentration in the ink, particle size and morphology in combination with the printhead. Secondly, the reliability and print consistency in a pharmaceutical context requires a careful long-term testing of the system alongside quality control. Thirdly (and maybe most importantly) there is a need of application and cost effectiveness for implementing industrial printing of pharmaceuticals. There is currently a shift in the trends for the pharmaceutical sector, where there is a demand on a broader range of flexible, specialized products in lower volumes for specific patient populations (and towards personalized medicines) that will not be fulfilled with traditional large-scale batch production. The new emerge of therapy areas as well as new technologies has potential for dramatic changes in pharmaceutical and medical manufacturing as well as in the supply chain. [3] [31]

In the beginning of 21st century, additive manufacturing (also referred to as 3D-printing) of pharmaceuticals with inkjet printing has focused on different powder-bed technologies, where a binder (ink) is printed on a powder layer-by-layer to build a macroscopic solid structure. The API can be placed in either the powder or the binder and final solid structure is then usually achieved by thermal sintering, which also limits the use of delicate functional pharmaceutical molecules. [32] [33] [34]

A huge historical breakthrough was in 2015, when Food and Drug Administration (FDA) approved the New Drug Application (NDA) for SPRITAM® (levetiracetam), the first 3D printed pharmaceutical product on the market (2016). The producer, Aprecia Pharmaceuticals Company, uses a ZipDose® technology to produce a porous orodispersible, anticonvulsant tablet for epilepsy. The ZipDose® technology is principally inkjet-printed layers of an ink binder and a powder, forming a mold for the tablet. The mold is then filled with an API-containing powder (up to 1 000 mg of API per tablet) and sealed with inkjet-printed layers of ink binder and powder. [1]

In contrast to standard inkjet printing and biological printing research where systems are usually modelled with a standard of glucose oxidase and Newtonian liquid such as water-glycerol mixtures prior to more complex experiments, there is no standard molecule to model APIs in inkjet printing of pharmaceuticals. However, a general trend of printing small molecules is yet noticeable (see

Table 1). The chemistry of APIs differs widely and is crucial for both ink formulation and ancillary printing equipment. According to Strickley, APIs from the same family behave similarly in carrier fluids and it was suggested by Daly *et al.* that the concept systems for printing pharmaceutical should focus on developing model systems so that it would be easier to apply an already working system to another, similar product. [3] [35]

Most pharmaceutical printing have been done with research scale printheads such as MicroDrop and Microfab single nozzle, PIJ glass capillary devices, Dimatix Material Printers, or modified consumer desktop printers. These have been studied due to their precise dosing and applicability for personalized medicine. Printed pharmaceuticals are expected to revolutionize drug preparation and it is envisioned that printers could be used in hospitals or pharmacies for late-stage customization. [3]

In Table 1, previously inkjet-printed APIs are summarized. Most APIs have been printed on thin films, sheets forms or tablets. Usually porous substrates such as hydroxypropyl methylcellulose (HPMC) have been used, but some cases where non-porous films and glass plates have been used are also noted. The inks were formulated according to API, printer and application.

Table 1. Summary of previous inkjet-printed APIs. (Modified from H. Wikström [9])

API	Print method	Reference
Acetaminophen	DoD	[36]
Caffeine	PIJ	[37]
Caffeine	PIJ	[38]
Cidofovir Paclitaxel	PIJ	[39]
Clonidine	TIJ	[40]
Diclofenac sodium	TIJ	[41]
Enalapril maleate	PIJ	[42]
Fenofibrate	PIJ	[43]
Folic acid	DoD	[44]
Glimepiride	DoD	[45]
Griseofulvin	EHD	[17]
Haloperidol	PIJ	[46]
Ibuprofen	EHD	[17]
Loperamide	PIJ	[38]
Lysozyme	TIJ	[47]
Mefenamic acid	DoD	[36]
Naproxen	DoD	[48]
Naproxen	DoD	[49]
Naproxen	DoD	[50]
Naproxen	PIJ	[51]
Paclitaxel	PIJ	[52]
Paracetamol	PIJ	[37]
Phenylbutazone	DoD	[36]
Piroxicam	PIJ	[53]
Piroxicam	PIJ	[54]
Prednisolone	TIJ	[55]
Propranolol hydrochloride	PIJ	[56]
Ramipril	DoD	[45]
Rasagiline mesylate	TIJ	[57]
Salbutamol	TIJ	[58]
Sodium picosulfate	PIJ	[59]
Sodium picosulfate	PIJ	[60]
Theophylline	PIJ	[37]
Thiamine hydrochloride	PIJ	[61]
Thyroxine (T4)	TIJ	[62]
Triiodothyronine (T3)	TIJ	[62]
Warfarin sodium	PIJ	[63]
Warfarin sodium	TIJ	[64]

Characterization of inkjet-printed pharmaceuticals is essential for product and application development. Characterization techniques and examples on practical implementations for inkjet-printed samples are listed in Table 2. Since inkjet printing is considered to be a precise dosing technique with an accuracy on microscale, it has potential to work as a method for preparing calibration standards for both already existing and new characterization technologies.

Table 2. Characterization techniques and examples of use in inkjet-printed pharmaceuticals. [3]

Characterization technique	**Objective**
Differential scanning calorimetry (DSC)	Verify crystallinity [65]
Thermogravimetric analysis (TGA)	Water content analysis [66]
Dynamic vapor sorption (DVS)	Crystallization behavior under humidity [66]
High-performance liquid chromatography (HPLC)	Drug release rate from stent [67]
Content analysis	Quantity of pharmaceutical in printed area [65]
Second harmonic generation (SHG)	Analyze the surface of crystal forms [68]
Energy-dispersive X-ray spectroscopy (EDX)	Distribution of API in sample [54]
Fourier transform infrared spectroscopy (FTIR)	Confirming co-crystal formation [69]
Ultraviolet–visible spectroscopy (UV–vis)	Verify dose in real time [31]
Raman spectroscopy	Polymorph identification [55]
X-Ray diffraction (XRD)	Polymorph identification [55]
Near-infrared spectroscopy (NIR)	Verify dose in real time [31]
Mass spectroscopy	Analysis of degradation products [37]
Time-of-flight secondary ion mass spectrometry (TOF SIMS)	Analysis of chemical heterogeneities [70]

2.2 Ink and substrate properties

2.2.1 Importance of ink formulation

Printable inks are under constant development and to this day, there is no universal ink that would fit every application. Print quality, image robustness, compatibility, application performance, jetting characteristics, adhesion, drying/curing process, pre- and post-processing, reliability, shelf life, manufacturing complexity, regulatory (i.e. FDA) are some main features that need to be taken into consideration when developing an ink for printing. Due to the scope of this thesis, the focus is concentrated on the desired physicochemical properties of printable API-containing inks.

An ink can contain solids either as dissolved in the ink solution or as colloidal particles (widely used to print metals and ceramics). In case of dissolving solids (APIs) into an ink, the loading is limited by the solubility of the solids in the ink. The ink composition and solvents can be tuned according to desired solubility, but this will also most likely affect other properties of the ink. Volume fraction of solids that can be used in an ink fluid is normally relatively low and heavily loaded colloidal fluids for printing are still under development. Not only does a colloidal ink suspension need to have the right rheological properties for printing, the size of the particles needs to be controlled to avoid nozzles from clogging. [8]

Regarding inkjet printing, surface tension and viscosity are the two most important properties for a printable ink. Liquid, printed from a circular nozzle, automatically takes a cylindrical, column shape. However, according to the law of Rayleigh-Plateau instability, surface tension causes the liquid to pinch off into smaller droplets to achieve energy minimum. Without interacting electrostatic or aerodynamic forces, the jetted liquid takes the shape with the lowest total energy, a sphere (see chapter 2.1.3) [8]. Liquid printed on a solid substrate interacts with the surrounding air and the substrate. The droplet's spreading on the surface is called wetting and it is a result of surface tension, cohesive forces within the liquid and the adhesive forces between the liquid and surface (solid) (see Chapter 2.2.3).

Viscosity, especially the dynamic viscosity, affects the flow behavior of the ink. Viscosity is a result of the interactive forces between the liquid's molecules when sections of the liquid are moving relative to one another. Viscosity is also related to the density of the liquid. Organic solvents (such as water and ethanol) are usually Newtonian and show a linear behavior under shear, but most practical inkjet inks are somewhat viscoelastic and show a time-dependent

elastic response to shear. The viscosity of most liquids is temperature-dependent and decreases with increased temperature. This is utilized in e.g. TIJ printing and temperature is often an adjustable feature for PIJ actuation. Thus, by adjusting the jetting temperature, the desired viscosity for printing ink might be achieved. [8]

Both surface tension and viscosity of the ink need to be appropriate to accomplish a good print quality. With too low surface tension and viscosity, there is a risk that the ink will run out of the nozzle by itself and with a too high surface tension and viscosity, the actuation force will not be strong enough to push the ink from the nozzle orifice. Both surface tension and viscosity can be controlled by addition of surfactants, humectants (normally some kind of glycol) and by selecting a proper solvent composition. Magadassi recommends an ink with viscosity 1-5 cP or 10-14 cP, density 0.9-1.1 g/ml and surface tension 20-50 mN/m for PIJ printing. The ranges can vary widely according to printer. Nozzle design, actuation technique, printing temperature and ink formulation are all factors that set the requirement for the ink's surface tension and viscosity. [7] [8]

2.2.2 Characteristic dimensionless numbers for ink formation

When a droplet is formed, surface tension, viscosity and inertia are the key properties for how the liquid behaves. Dimensionless numbers have been developed to theoretically describe a liquid's behavior. The three most relevant parameters for droplet jetting are presented in this chapter. The Reynolds (Re) number describes the relation between viscous and inertial forces of a moving fluid, while the Weber (We) number represents the influence of kinetic energy in relation to surface energy. By combining these two into the Ohnesorge (Oh) number, the influence of velocity can be eliminated. [8] [71]

$$\boldsymbol{Re = \frac{\rho d V}{\eta}} \quad \textbf{Equation 1.} \qquad \boldsymbol{We = \frac{\rho d V^2}{\sigma}} \quad \textbf{Equation 2.} \qquad \boldsymbol{Oh = \frac{\sqrt{We}}{Re} = \frac{\eta}{\sqrt{\sigma \rho d}}} \quad \textbf{Equation 3.}$$

ρ is the density of the fluid, V the velocity, η the viscosity, σ the surface tension and d describes a characteristic length, normally the diameter of the nozzle, jet or droplet. Oh number describes how a jet emerges from a nozzle, taking into consideration the physical

properties of the liquid and the size of the jet or droplet [20]. With an Oh number close to 1, the viscous forces will prevent a droplet from separating from the liquid in the nozzle but if the Oh number is too low and close to 0.1, the liquid will form satellite drops (see Chapter 2.1.3). In DoD printing, all the parameters, including velocity, still must be optimized to achieve a suitable combination of physical properties for printing. Fromm opined that an ink with Oh number lower than 0.5 should be printable with DoD printing, this while the optimal parameters for printing are suggested to be to 0.1<Oh<1 according to e.g. Reis and Derby among others and 0.07<Oh<0.25 according to Jang *et al.* [12] [20] [72] [73]. Magadassi suggests an ink with Re number 50-500 and We number 20-300 for inkjet printing [7].

Inkjet printing usually has droplet volumes up to 200 pL and inertial effects are more significant than the effect of surface energy and viscosity. This means that the Re and We numbers can be high while Oh number is low and that the exchange between surface and kinetic energy is the most relevant factor in printing. The Re, We and Oh number are developed for Newtonian fluids and while they are indicative for if a printing will succeed, the rheology of printing inks (e.g. shear-thinning or viscoelastic behavior), printhead design and surrounding factors might differ and, therefore, the best way of assuring good printability is through experimental tests. [8]

2.2.3 Correlation between ink and substrate

While drop-substrate interactions have been studied extensively by Worthington (1876), Armster *et al.* (2002) and Yarin (2006) among others, a complete explanation of the complex flow mechanisms has not yet been done [8]. The mechanisms include the droplet's kinetic energy that initiates spreading on the surface until this energy is converted to surface energy or lost through viscous dissipation. Factors such as initial mass and velocity of the droplet, surface tension and viscosity of the fluid and properties of the substrate are essential for explaining the drop-substrate behavior. Some theories have been presented, trying to explain the liquid-solid interactive behavior (wettability) and some dimensionless numbers have been established to describe a liquid's viscous, inertial and surface forces. Three of these are presented in Chapter 2.2.2.

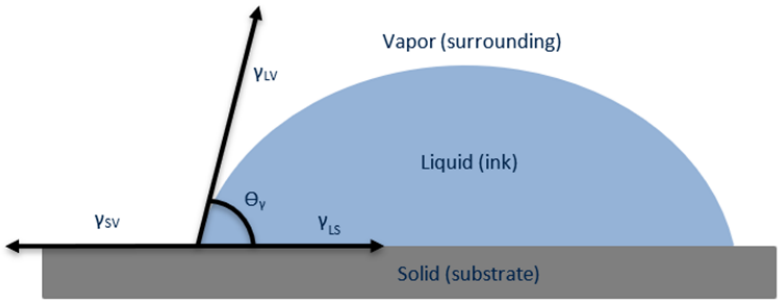

Figure 4. A liquid drop in equilibrium on a surface with contact angle (Θ_γ) depending on three surface energies: liquid-vapor (γ_{LV}), solid-vapor (γ_{SV}) and liquid-solid (γ_{LS})

A drop rests in equilibrium on a surface with an equilibrium contact angle, Θ_γ (also referred to as Young contact angle), which is dependent on three prominent surface energies: surface energy component (γ_{LV}) which is the interfacial surface tension between the liquid and the vapor, surface energy component (γ_{SV}) which is the interfacial surface tension between the solid and the vapor, surface energy component γLS (γ_{LS}) which is the interfacial surface tension between the liquid and the solid (see Figure 4). The surface free energy (SFE) for a solid is given by Young equation (4) [74].

$$\boldsymbol{\gamma_{SV} = \gamma_{LS} + \gamma_{LV} \cos \theta_\gamma} \qquad \textbf{Equation 4.}$$

The equation assumes that the surface is homogeneous and has a smooth topography. The contact angle (Θ_γ) and liquid-vapor surface tension (γ_{LV}) are easily determined, but the solid-liquid surface tension (γ_{LS}) cannot be measured directly without assumptions. Since the measuring liquid and interfacial interactions with the substrate play an essential role in the determination of γ_{LS}, Fowkes suggested that the SFE should be calculated as a sum of dispersive, polar, hydrogen, induction components and additionally a component including remaining interactions [75]. Owens, Wendt, Rabel and Kaelble simplified the idea and supposed that the components could be considered either dispersive (γ^d) or polar (γ^p) and combined this theory with Young equation into so called OWRK equation (5) [76].

$$\sqrt{\boldsymbol{\gamma_{SV}^d \gamma_{LV}^d}} + \sqrt{\boldsymbol{\gamma_{SV}^p \gamma_{LV}^p}} = \boldsymbol{0.5 \gamma_{LV}(1 + \cos \theta_\gamma)} \qquad \textbf{Equation 5.}$$

A further, more resent approach is the Van Oss-Chaudhury-Good (vOCG) method where the polar components are divided into acid and base components and the equation is written as (6) [77].

$$\sqrt{\gamma_{SV}^{d}\gamma_{LV}^{d}} + \sqrt{\gamma_{SV}^{acid}\gamma_{LV}^{base}} + \sqrt{\gamma_{SV}^{base}\gamma_{LV}^{acid}} = 0.5\gamma_{LV}(1 + \cos\theta_{\gamma}) \qquad \textbf{Equation 6.}$$

Since the equation includes three unknown components, γ_{SV}^{d}, γ_{SV}^{acid}, γ_{SV}^{base}, at least three measuring liquids are needed, one dispersive and two polar, to calculate the SFE for a surface.

The Young contact angle is a simplification and considers the measuring surface as ideal and disregards both the apparent and the actual contact angle which consider surface roughness [7]. Real surfaces often show some extent of roughness or/and chemical heterogeneity and can be measured to some degree with various methods. Roughness is an important factor for understanding wettability of a surface, but it is considered to extend the scope of this thesis and is therefore not covered in this work.

2.2.4 Typical limitations and challenges for printing

When designing a printing sequence, the main print-influencing factors that need to be taken into consideration are following:

- Ink suitability for the print function
- Ink-printer material compatibility (both short and long term)
- Printability of ink in the specific printhead
- Reliability of ink for print consistency
- Ink-substrate adhesion behavior
- Substrate consistency (substrate might need pretreatment)
- Drying and/or curing process (can also be improved with post-treatment)
- Printing environment (temperature, humidity, contaminants, dust…) [8]

Nozzle clogging is a feature that, most probably, ruins the print result to some extent. Nozzles can clog due to ink solvent evaporation at the tip of the nozzle, or due to too large particles in the ink. Less volatile solvents with lower evaporation rate are usually preferred in inks. Another option is to add a co-solvent to delay loss of e.g. water by hydration. Often used humectants are different types of glycols. Solids need to be soluble in the ink solution (this can be maximized by changing the ink solvent composition) or stable as colloidal particles of the right size. [7]

Solvent evaporation can also cause changes in the ink properties such as solubility and viscosity (viscosity usually increases because of evaporation). The time that an ink can successfully wait in an orifice without being jetted is called latency and this can vary from seconds to several minutes, depending on ink [7]. Usually, inkjet printers have built-in maintenance with nozzle-cleaning cycles with spitting and purging effects, where the nozzle is cleaned from any unwanted substance in the nozzle [8]. Some printers (e.g. Dimatix Materials Printer DMP-2800 Series), apart from a jetting wave form for print droplets, also have a non-jetting wave form, "tickle control". The non-jetting pulse signal is sent to the printhead while it is moving in between printing of droplets and keeps the ink in the nozzle in motion and prevents it from drying [15].

The ink's behavior on the substrate is another factor that might ruin the quality of the print. On top of a non-porous substrate, the ink droplets might cause "clusters" in case of under-wetting and a high dot-gain. In case of too high speed of the jetted droplet, a splashing effect might occur when the droplet hits the substrate. This is a result of when the rheological properties of the ink do not match the rest of the printing set-up. The jetting speed can be adjusted by the power of the piezoelectric impulse and the distance between the printhead and the substrate. [7] [8]

3 MATERIALS AND METHODS

3.1 Ink preparation and analysis

3.1.1 Theophylline

Anhydrous theophylline (Theophylline Anhydrous 200M, Orion Corporation) was used to model APIs on different surfaces. Theophylline (1,3-dimethyl-xanthine) (see Figure 5) has been used for 80 years. It is the most prescribed drug for airway diseases treatment and is included in the World Health Organization´s (WHO) core of essential medicines. The molecule is small, poorly water-soluble and forms slightly acidic solutions in water. Theophylline easily undergoes hydrate–anhydrate pseudopolymorphic transformations and shows a cocrystallization behavior to form crystalline molecular complexes. This significantly affects its solubility, stability and bioavailability. [78] [79]

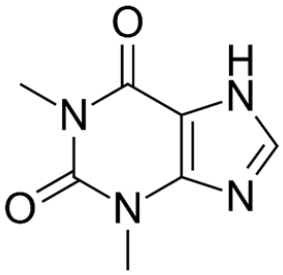

Figure 5. Theophylline molecular structure

3.1.2 Ink preparation

The inks were prepared by dissolving a known amount of theophylline (API) powder in a known volume of purified water (W) and was magnetically stirred (250 rpm) for 30-60 min at room temperature. If the API did not dissolve, the solution temperature was increased to 50 °C and magnetically stirred for another 30 min. The co-solvents and additives, ethanol (EtOH) (Spiritus Fortis / Ethanol 96%, Orion Corporation), glycerol (G) (Orion Corporation) or propylene glycol (PG) (Orion Corporation) were added in known amounts and the solution was magnetically stirred for yet another 15-60 min. Corresponding placebo inks, without API, were also prepared. The final ink compositions and API concentrations are listed in Table 4.

3.1.3 Density

An Anton Paar DSA 5000 densitometer (DSA, Density and Sound Velocity Analyzer) was used to determine the density of the inks. The measurement cell uses an oscillating, thermostatic U-formed capillary tube to measure the oscillating frequency for the sample injected in the tube. The instrument was calibrated with cooked, ionized water and cleaned with purified water, ethanol, acetone and pumped dry with the built-in air dryer for 5 min in between samples. Ink sample (5 mL) was injected in the capillary tube and the measurements were performed in 25 °C.

3.1.4 Viscosity

The viscosity of the inks was measured with an Ostwald viscometer. The Ostwald U-tube measures the liquid's running time (*t*) through a capillary tube from one point to another. The running time is compared with a standard liquid's running time from where the viscosity constant, *k*, is calculated. The viscosity, *η*, can be calculated if the liquid's density, *ρ*, is known.

$$\boldsymbol{\eta = k \cdot \rho \cdot t} \qquad \textbf{Equation 7.}$$

The viscosity measurements where performed with a U-tube with viscosity constant *k*=0.016 (mPa*m^3)/g. The U-tube was injected with 3 mL of ink sample and stabilized in a water bath, 25 °C for 5 min. The sample was prepared with a suction blub and the timer was managed by hand. The tube was cleaned with purified water, ethanol, acetone and pressurized air. Each ink was tested three times and a mean value for the running time was calculated.

3.1.5 Surface tension

Two types of tensiometers were used to determine surface tensions for the inks, a so-called bubble tensiometer and a ring tensiometer.

Maximal Bubble Pressure was measured with SensaDyne (PC9000) which uses the Young-Laplace equation to calculate surface tension. Two capillary tubes were submerged in the

sample and a gas bubble was blown under the liquid surface. By knowing the diameter of the capillary tubes, which will be the same as the diameter of the bubble, the maximum pressure can be measured. By using two capillary tubes on slightly different levels, the effect of hydrostatic pressure can be eliminated. The advantage with the Maximum Bubble Pressure Method is that it measures both dynamic and static surface tension. [80]

The instrument was calibrated with cooked, distilled water and ethanol (Aas quality). An ink sample of 100 mL was prepared in a beaker and measured three times in room temperature (21-22 °C). A mean value for the ink's surface tension was calculated. The tubes were cleaned with water and ethanol in between samples.

The ring tensiometer, KSV Sigma 70, measures the maximum force with which a Pt-Ir circular torsion wire is pulled from a liquid surface. The method is certainly sensitive for surface active molecules in the phase boundary layer between the sample liquid and air.

The instrument was calibrated, and the measuring ring rolled into an even circle and burned from potential residuals and impurities and cleaned with purified water, ethanol and acetone. Ring measurement settings were set to Speed Up: 5.0 mm/min, Speed down 20.0 mm/min, Dwell Down 5.0%, Min No of Points 3, Min Meas. Time: 1.0 and Autozero. The measurements were performed with 40 mL of sample in the small vessel in room temperature, 21 °C. The vessel was washed with water, ethanol, acetone and pressurized air in between the measurements.

3.1.6 Particle size

Particles size in the printing inks was measured with Dynamic Light Scattering (DLS), with a Malvern Zetasizer Nano-ZS ZEN 3600 instrument. The instrument measures sub-micron sized particles dispersed in a liquid by exposing the sample for a laser beam (632 nm). By measuring the intensity of the scattered light, the velocity of the Brownian motion in the particles can be determined, and according to Stokes-Einstein equation, the translational diffusion coefficient and furthermore the particle size can be determined, with the assumption that the particles have spherical shape.

The sample was prepared by injecting the ink sample into a UV grade cuvette (10-15 mm). Measurements were performed with theophylline as material (refraction index (RI) 1.7 and absorption 0.01) and dispersant according to the different ink composition. Primary solvent

was set to water and the concentrations of the other ink components were added according to their calculated concentrations (mol/L) in the ink. The software calculated the RI and viscosity increment and the final, theoretical RI and viscosity of the ink-liquid. The measurements were performed three times at 25 °C.

3.2 Printing

3.2.1 Dimatix DMP 2830 Material Printer

The printing experiments were performed with a FUJIFILM Dimatix DMP 2830 Material Printer and associated cartridges for the inks (see Figure 6). The disposable 10 pL droplets cartridge (model # DMC-11610 / PN 210020146) was injected with 1.5 mL of ink.

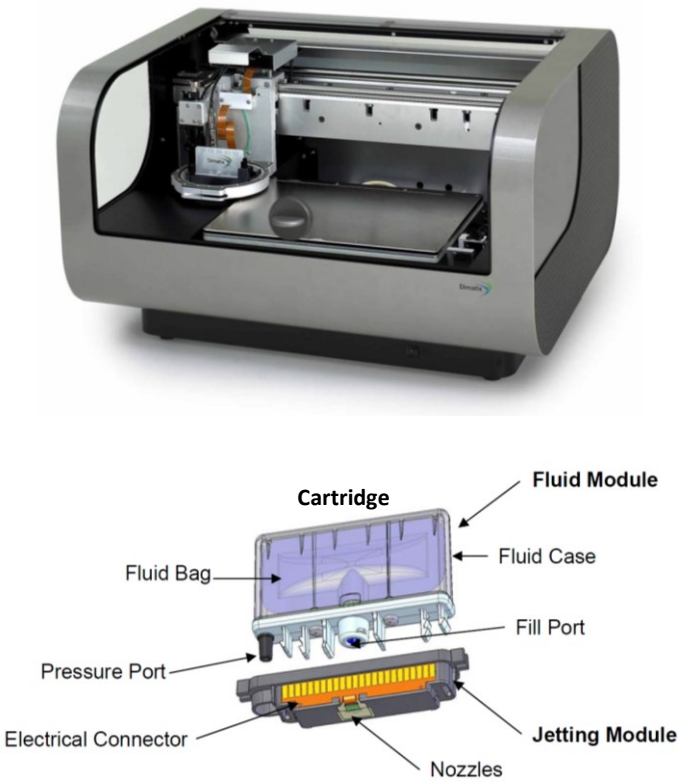

Figure 6. Dimatix Materials Printer DMP-2800 Series and associated ink cartridge. [15]

The cartridge has an ink pumping chamber, a fluid inlet passage with 16 individual nozzles, spaced 256 µm apart which actuate and dispense the ink with a piezoelectric transducer. The nozzles have 21.5 µm openings and the firing voltage and the waveform are user controlled for each nozzle [15]. A "caffeine" waveform-setting (see Figure 7) was selected, since theophylline has previously been printed with this waveform. Cartridge settings were set to "no set temperature", meniscus vacuum setpoint to 5.0 inches and "H20Print". Cartridge print height was set to 0.850 mm.

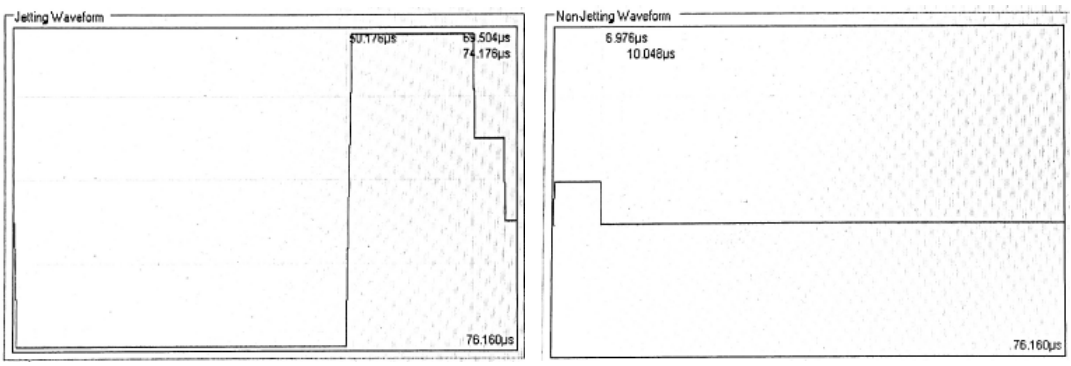

Figure 7. "Caffeine" jetting waveform and non-jetting waveform (tickle control). The jetting waveform is constructed as a ramp to dispense the ink liquid into spherical droplets. Tickle control prevents the liquid from drying at the nozzle orifice in between ejected droplets.

A series of 1 cm^2 × 1 cm^2 square patterns with different drop spacings were edited and the cartridge angle was adjusted manually according to the printer's recommendations. The ink was stabilized in the cartridge, attached to the printhead for one hour before printing. The ink droplet firing temperature and the temperature of the substrate were not adjusted. The firing voltage was set to 13-15 V to obtain optimized droplets (see Chapter 2.1.3) according to the ink's specific properties (surface tension, viscosity and API loading). The droplet firing was observed with the drop-watcher function of the printer. One printing nozzle was selected for printing. The height of the substrate was set according to the substrate and vacuum was used to induce negative pressure in the printer. Printed samples were dried in a vacuum oven, 60 °C, pressure 1-10 Torr overnight to evaporate the solvents from the ink, leaving only API on the substrate.

3.2.2 Printing substrates

Eight different printing substrates were used. Stainless steel, plexi, aluminum, epoxy (floor material) and rubber (production sealant) test plates were received from Orion Corporation, glass (Microscope Slides T/F Ground 1.0 mm, Fisher Scientific Oy) and paper (A4 copy paper, Staples Europe B.V.) from Åbo Akademi University and enamel test plates (Glass-lines samples, DD3009 blue plate, De Dietrich) from Thurne Teknik AB. The substrates are commonly used materials in drug production facilities and paper was used as reference substrate.

3.2.3 Surface energy of printed substrates

The SFE for the substrates was calculated from the determined contact angle of three liquids with known surface tension, and the OWRK and vOCG theories presented in Chapter 2.2.3. The used dispersive liquid was diiodomethane (DIM), and water and ethylene glycol (EG) were used as polar liquids. The contact angles were measured with a KSV CAM200 goniometer (KSV Instruments Ltd.) and associated software. KSV's CAM 200 is a computer-controlled instrument which measures surface free energies, surface or/and interfacial tensions of liquids, static and dynamic contact angles and absorption of liquids into porous materials by video capturing and automatic image analysis based on Young-Laplace and Bashforth-Adams theory.

Drops of 2 µL (EG and water) and 1.4 µL (DIM) were dosed by an automated syringe and placed on the substrate manually with placer-screw. Then 25 pictures were taken with one second interval from the moment the drop touched the surface and the contact angels were calculated by the software. The experiment was repeated five times and a mean value for the contact angle was plotted over time. One contact angle per each liquid on each substrate was determined to be the stable equilibrium contact angle. Since the dispersive and polar (acid-base) components for the liquids were known from the literature (listed in **Table 3**), the vOCG and OWRK theories could be used to determine the SFE for the substrates.

Table 3.Total surface tension (γ^{tot}) as well as the dispersive (γ^{d}), polar (γ^{p}), acid (γ^{acid}) and base (γ^{base}) components of surface tension in mN/m for DIM, EG and water found in the literature. [77]

	γ^{tot}	γ^{d}	γ^{p}	γ^{acid}	γ^{base}
DIM	50.8	50.8	-	-	-
Water	72.8	21.8	51.0	25.5	25.5
EG	48.0	29.0	48.92	1.92	47.0

3.3 Analysis of the printed samples

3.3.1 Optical analysis

The reference substrates and the samples were visually analyzed with a USB microscope, Dino-Light Digital Microscope (N3C-O / Open Cap). The actual drop spacing was measured using the measuring tool in the associated software, DinoCaptue 2.0 Version 1.5.39.C (AnMo Electroics Corporation 2016).

3.3.2 Near infrared spectroscopy

A two-piece handheld NIR reflection spectral device N2.0 (Spectral Engines Oy) was used to perform NIR measurements. The two units measure the absorbance spectra in the wavelength range of 1.35-1.65 µm and 1.55-1.95 µm. Each unit has a single element indium gallium arsenide (InGaAs) detector and the illumination orifice (Ø 1 mm) is made of two tungsten vacuum lamps. The instrument is never in direct contact with the sample, the measurements are simply made from a 2 mm distance from the surface. [81]

Before starting the measurement, dark signal and reference of the clean substrate was collected. Sample data was collected from 12 different spots from 4 parallel printed samples. The illumination lamps were set to 50% or 100% of the lamps' maximum voltage and the data was collected with 5 nm steps throughout the range of wavelength.

3.3.3 Infrared spectroscopy

Infrared (IR) spectra were measured with a Nicolet iS50 Spectrometer (Thermo Fisher Scientific Inc.), which is a multirange FTIR spectrometer that has a wide range of different applications. An iS50 ATR Module with single-bounce and single detector configuration was used for Attenuated Total Reflection (ATR) IR measurements. The module consists of a diamond ATR crystal (Ø 5 mm) and a pressure tip with which the sample (e.g. plates, powders, or liquids) is fastened.

3.3.4 Raman spectroscopy

The same Nicolet iS50 Spectrometer as for FTIR measurement was also used for Raman measurements. The instrument uses a non-exchangeable 1064 nm laser excitation source with a maximum power of 0.5 W, a Calcium fluoride (CaF_2) beam splitter and a dedicated InGaAs detector. The power was set to 0.05 or 0.5 W for the measurements.

4 RESULT AND DISCUSSION

4.1 Suitable ink for printing

The first issue to take into consideration regarding printing of drugs is the drug-containing ink. The carrier fluid can have different roles for the ink properties; these include 1) dissolving of the API 2) carrying phase for a colloidal dispersion 3) adjust evaporating properties of the ink. According to the literature, inkjet-printed pharmaceuticals often have a water-based carrier fluid [3]. Water has a viscosity of 1 mPa*s in room temperature, which is usually too low for printing and co-solvents or/and additives are usually needed. Daly presented that up to 40% of drug-printing candidates have been abandoned due to poor aqueous solubility [3]. The requirements for the ink in this work are that the API, in this case Theophylline, needs to be stable and preferably soluble in the ink fluid and that the ink needs to have the right properties for the printing technique and specific printer.

4.1.1 Suitable ink formulation for printing

Ethanol and water were chosen as solvents due to the solubility of theophylline in respective, 15.19 mg/mL and 7.36 mg/mL [82]. Pure ethanol would have been favorable for both solubility and for fast drying on the substrate, but to avoid the printing nozzles from drying and clogging, a slowly evaporating ink is preferred. The manufacturer, FUJIFILM Dimatix Inc., also suggests adding glycol to the ink to slow the evaporation [15]. Propylene glycol and glycerol were used as viscous additives, since both have previously been used in inkjet inks [37] [83]. Sandler *et al.* used propylene glycol in a theophylline-containing ink, and the ink formulation procedure was repeated and evaluated in this research (filtering excluded) [37].

It is possible to print inks with particles with the selected cartridges, but any particles should preferably be smaller than 0.2 µm which corresponds to 100 times smaller than the nozzle orifice [15]. It is suggested to filter the ink fluid through a 0.2 µm filter pre cartridge loading [15]. Despite that, this step was neglected due to the crucial aspect of printed API concentration in this research.

For surface tension measurements, two instruments were evaluated: a ring tensiometer and a bubble tensiometer. The measurements slightly differed from each other, indicating that some component in the inks was somewhat surface active. However, the maximum bubble

pressure method would be considered to model the droplet formation in the printing process and the droplet impact on a solid surface and was therefore chosen as the method for surface tension measurements [84]. Magadassi suggests that the ring tensiometer could be a complement to the dynamic surface tension measured with a bubble tensiometer, but that the bubble method still models the droplet formation in the printing process more truthfully [7].

Altogether, 16 different inks were prepared, both with API and placebo. The inks were analyzed for surface tension (bubble tensiometer), density, viscosity and particle size. The results are summarized in Table 4. Viscosity was calculated with Equation 7, out of the viscosity constant of the Ostwald U-tube, the liquids´ density and the running time through the U-tube (see Chapter 3.1.4).

Table 4. Measured surface tension and density for the inks. The viscosity was calculated by Equation 7. The size of particles in the inks was measured and the dominating particle size for each ink are listed. All measurements were performed at 25 °C. The G:EtOH:W (10:45:45)-ink composition was determined to have the best properties for printing and was prepared with several different concentrations of API.

Ink composition	Surface tension (mN/m^2)	Density (g/cm^3)	Viscosity (mPa*s)	Particle size (nm)
PG:W (30:70) + API 5.8 mg/mL	53.2	1.02	3.78	1429
PG:W (30:70)	53.2	1.02	3.77	162
EtOH:W (30:70) + API 5.8 mg/mL	35.8	0.96	1.89	276
EtOH:W (30:70)	35.8	0.97	1.87	190
PG:EtOH:W (10:20:70) + API 5.8 mg/mL	39.6	0.98	2.07	310
PG:EtOH:W (10:20:70)	39.5	0.98	2.06	305
G:W (10:90) + API 5.8 mg/mL	72.8	1.03	1.10	135
G:W (10:90)	72.8	1.02	1.08	247
G:EtOH:W (10:10:80) + API 5.8 mg/mL	50.3	1.01	1.31	152
G:EtOH:W (10:10:80)	49.8	1.01	1.33	60
G:EtOH:W (10:45:45) + API 0.06 mg/mL	30.8	0.96	2.97	215
G:EtOH:W (10:45:45) + API 0.23 mg/mL	30.8	0.96	2.93	231
G:EtOH:W (10:45:45) + API 0.48 mg/mL	30.7	0.96	2.97	251
G:EtOH:W (10:45:45) + API 5.80 mg/mL	30.3	0.96	2.98	272
G:EtOH:W (10:45:45) + API 11.84 mg/mL	31.0	0.98	2.98	172
G:EtOH:W (10:45:45)	30.3	0.96	2.91	253

As seen in Table 4, surface tension of the different ink compositions differs. Surface tension of an API-containing ink and the corresponding placebo ink was similar. Ink densities were about 1 g/cm^3 for all ink compositions. Running time in the Oswald viscosimeter differed widely among the inks, which indicates different viscosities of the inks. A trend where water content relates to a higher surface tension was observed. The results also show that with increasing amount of ethanol, the surface tension decreases and viscosity increases. It is also noticeable that flocculation and particle aggregation displays as increased viscosity [7].

All inks, both API-containing and placebo, contained particles to some extent. Apart from aggregated theophylline, the particles could have occurred in the solvents and/or additives used in the inks or be contaminants, such as dust from the air. It was yet obvious that there in some of the ink compositions had occurred some particle formation. A cloudiness was observed in the PG:W-ink fluid containing API and DLS measurements also confirmed that the ink contained particles bigger than 1400 nm. Since filtering was avoided in this research (unlike in the Sandler research group [37]), glycerol was preferred as an additive in the inks, since it barely showed signs of particle aggregation.

The manufacturer's recommendations for ink viscosity and surface tension is 1-40 mPa*s (preferably ca. 10 mPa*s) and 28-33 mN/m^2 respectively [15]. Particle size is suggested to be under 200 nm (100 times smaller than the nozzle orifice) [15]. None of the prepared inks fulfilled all criteria, however, it was suggested to test print the G:EtOH:W (10:45:45)-inks, since surface tension met the criteria for printing and the particle size was just slightly over 200 nm. The printings proceeded successfully although all the criteria were not fully met. G:EtOH:W (10:45:45)-ink containing theophylline was slightly acidic (pH 6 measured with pH paper), while the corresponding placebo ink was neutral (pH 7).

4.1.2 Calculated Re, We and Oh numbers

The characteristic numbers for droplet formation, Re, We and Oh numbers, for the different ink compositions were calculated by Equation 1, 2 and 3 presented in Chapter 2.2.2, and summarized in Table 5. Apart from some particle formation, the physicochemical properties of the higher API-containing inks did not differ significantly from the corresponding placebo ink and therefore is was decided to only calculate the characteristic numbers for the placebo ink compositions. The measured surface tensions, densities and viscosities of the inks are presented in Chapter 4.1.1, Table 4. The characteristic length, *d*, was set to the orifice diameter of the printing nozzle, 21.5 µm. Since the velocity of the printed droplet was unknown, but assumed to be between 7 and 9 m/s according to Dimatix's recommendations, an interval for Re and We numbers was calculated for each ink where minimum refers to a velocity of 7 m/s and maximum to 9 m/s [15]. The Oh number can be calculated without knowing the velocity (see Chapter 2.2.2).

Table 5. Re, We and Oh numbers calculated by Equation 1, 2 and 3. Ink velocity is assumed to be 7-9 m/s.

Ink composition	Re	We	Oh
PG:W (30: 70)	41-52	20-33	0.11
EtOH:W (30:70)	78-100	29-47	0.07
PG:EtOH:W (10:20:70)	72-92	26-43	0.07
G:W (10:90)	143-183	15-24	0.03
G:EtOH:W (10:10:80)	115-148	21-35	0.04
G:EtOH:W (10:45:45)	50-64	33-55	0.12

The Re, We and Oh numbers of different ink compositions vary broadly because of their different surface tensions, densities and viscosities. Figure 8 is a theoretical overview of "printability" of the inks according to the characteristic numbers. The solid diagonal line corresponds to Re=2/Oh and the kinetic energy of the jet ejected from the nozzle, while the broken diagonal line corresponds to OhRe5/4=50 and the droplets impact on the substrate (to avoid splashing) [3]. According to this theory, two of the ink compositions, PG:W (30: 70) and G:EtOH:W (10:45:45), have the right properties for printing. However, in the API-containing PG:W (30: 70)-ink, theophylline was found to aggregate to bigger particles (1400 nm) and the ink is therefore not printable with the printer. The G:EtOH:W (10:45:45)-ink composition was concluded to have the right physicochemical properties for printing and was used throughout this work and is hereafter referred to as the "optimized ink composition".

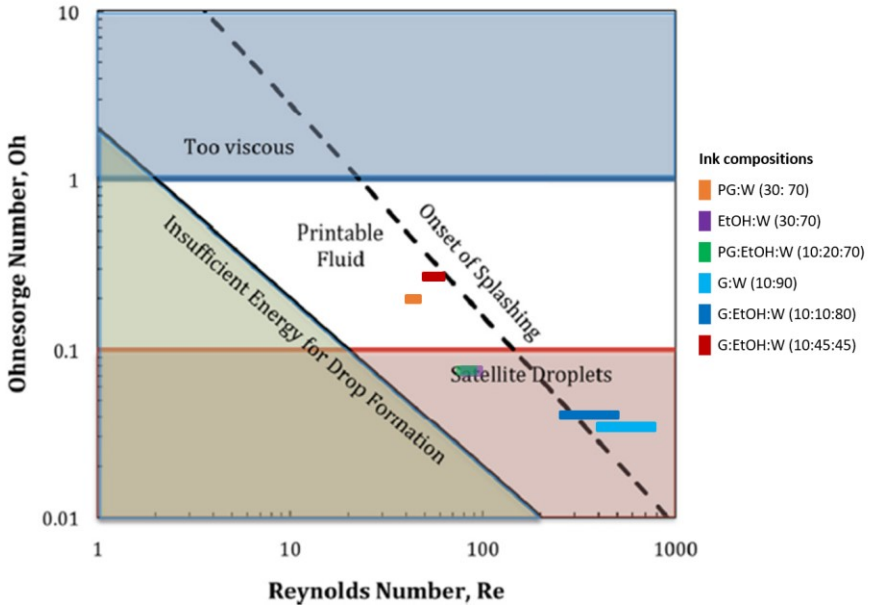

Figure 8. A theoretical overview of "printability" of the prepared inks according to their calculated Re and Oh numbers. (Modified from Hutchings *et al.* [8])

4.1.3 Surface energy of substrates

The equilibrium contact angle for three different liquids was measured for each substrate. Water and EG were used as polar liquids and while water has bipolar properties and equally big acid-base components, the base component of EG is significantly larger than the acid component (see **Table 3**). DIM was chosen as dispersive liquid.

All substrates except paper were non-absorbing and the measuring liquid stayed on the surface for the whole measurement and the equilibrium contact angles were determined without difficulties. Paper, however, absorbed all the three measuring liquids during measurements and an equilibrium contact angle was therefore somewhat problematic to determine. vOCG and OWRK methods (Equation 5 and 6) were used to calculate the $\gamma_{SV}^{\boldsymbol{d}}$, $\gamma_{SV}^{\boldsymbol{p}}$, $\gamma_{SV}^{\boldsymbol{acid}}$, $\gamma_{SV}^{\boldsymbol{base}}$ and the surface energy SFE for respective samples. The values are listed in Table 6.

Aluminum was determined to have a significant higher SFE than the rest of the substrates, plexi, paper, epoxy, steel and enamel all have similar SFEs, while glass and especially rubber have a significant lower SFE. Aluminum, enamel and glass (especially enamel and glass) were noted to have significantly higher values for base and polar component.

Table 6. Measured contact angles and calculated γ_{SV} for DIM, water and EG on the different substrates. The contact angles are given in degree (°) and surface tension components in mN/m. SFE was calculated with vOCG and OWRK methods (Equation 5 and 6).

	DIM Θ_Y	γ_{SV}^{d}	H_2O Θ_Y	γ_{SV}^{p}	EG Θ_Y	γ_{SV}^{acid}	γ_{SV}^{base}	Total SFE
Aluminum	47.5	35.7	32.4	30.2	72.8	6.5	27.3	62.3
Plexi	34.2	42.4	76.6	4.1	62.9	1.4	2.8	46.4
Paper	34.3	42.3	73.5	5.3	53.5	0.4	6.7	45.7
Epoxy	32.6	43.1	73.2	5.2	47.7	0.1	8.1	45.2
Steel	42.7	38.2	76.9	4.9	76.9	3.6	1.5	42.9
Enamel	40.5	39.4	27.0	30.7	23.5	0.03	58.9	41.8
Glass	49.1	34.8	42.5	25.0	32.4	0.01	48.4	36.3
Rubber	64.3	26.1	80.8	6.6	72.0	0.3	9.6	29.5

According to Magadassi, spontaneous wetting occurs when an ink has lower surface tension than the surface energy of the substrate [7]. The surface tension of the printed inks (with optimized ink composition) was about 30 mN/m and lower than the SFE of all the substrates except rubber. This results in larger dots (due to spreading) on the surface and a possibility of droplets merging in case of closely printed droplets (small drop spacing). Magadassi also

suggests that to achieve smaller printed dots, e.g. for a higher printing resolution, the surface tension should be high [7]. However, this thesis focuses on printed concentration of API on a surface, and not necessarily the visual outcome of printing. Surface tension and SFE can explain some specific behavior of an ink on a substrate (see Chapter 2.2.3), but a deeper understanding of ink-surface interactions is achieved with consideration of surface roughness. This is, however, considered to extend beyond the scope of this thesis.

4.2 Printing results

Inkjet-printed ink concentration can be adjusted in several ways. The focus of this thesis was amount of API per surface area. Taking into consideration that the droplet volume is standardized to 10 pL for the printing cartridges used in this work, three common ways of adjusting the printed API concentration per area are listed below. These methods were all investigated, with focus on adjusting the drop spacing, since it was determined to be the most efficient method for adjusting API concentration per surface area for this application.

1. Adjusting the drop spacing (Chapter 4.2.1). By having an ink with a known concentration of API, the amount of API on the printed area can be adjusted by the quantity of droplets. A larger drop spacing results in fewer droplets per area (lower dpi) and lower API concentration per area.
2. Adjusting the API concentration in the ink (Chapter 4.2.2). By changing the API concentration in the ink and printing with a set drop spacing, different API concentrations per area are achieved.
3. Printing several layers (Chapter 4.2.3). By printing several layers of API-containing ink, the API amount per area is increased. This method also allows printing large amounts of API, since it is neither restricted to solubility of the API, nor the printer's limitations.

All methods are followed by their own limitations and challenges. Adjusting the drop spacing (method 1) is limited by the maximum and minimum drop spacing of the printer. The printing result can differ, depending on the ink's wetting properties and the closeness of the printed droplets. Closely printed droplets tend to merge into bigger drops, due to the law of minimum surface tension and according to wetting on the surface (as a result of SFE). While the amount of API per printed area is easily adjusted, the amounts of ink solvents and additives are equally increased. This might affect printing results and analysis of the samples.

Adjusting the API concentration in the ink (method 2) is limited by the solubility of the API and by the crucial printing properties such as ink stability, viscosity, and particle size. Since the solvent-API ratio can differ, the solvent evaporation might vary depending on the ink. Limitations for layer printing (method 3) include slower printing process, especially if the first layer needs to dry before the second one is applied. Layer printing can affect the quality of the finished print and top-surface analysis might give inaccurate results in case of API concentration per area.

One single nozzle out of the 16 available in the cartridge was used for printing. This decision was made due to the crucial aspect of printed API. By printing with a single nozzle, it was possible to observe if the printing succeeded or if the nozzle clogged. This would not have been possible by using several nozzles at once (if one or some of the nozzles clogged, there would still be some ink printed on the substrate). Using several nozzles would, however, speed up the printing process.

4.2.1 Method 1: Printed API concentration adjusted with drop spacing

The optimized ink composition containing 5.8 mg/mL of Theophylline was printed on the eight different substrates with five different drop spacing settings, resulting in samples with five different printed API concentrations per area, listed in Table 7. Parallel with these, corresponding placebo samples without API were printed with the same drop spacing settings.

Table 7. Listed drop spacing, and associated number of droplets per square centimeter (given by the printer's software). The droplet size was standardized to 10 pL and the API concentration in the ink is 5.8 mg/ml from which the printed API per square centimeter was calculated.

Drop spacing (um)	Droplets per 1 cm^2	Printed API ($\mu g/cm^2$)
100	10 201	0.59
50	40 401	2.34
35	82 369	4.78
10	1 002 001	58.12
7	2 044 900	118.60

Due to the varying porosity and color of the substrate, some prints were impossible to detect optically (e.g. white paper as substrate). An alternative would have been to add a colorant to the transparent ink, like Vakili *et al.* did in 2017 [81]. This was not preferred in this work since the colorant could disturb spectrometric analysis. The API-containing inks, however, did turn white when dried due to the color of theophylline, and was visible on most of the darker colored substrates. As expected, the printed placebo samples were impossible to detect as water and ethanol had evaporated during drying.

Figure 9 and Figure 10 are microscopic pictures of the five different printed API concentrations per area on plexi and enamel, including a picture of the plain substrate reference. Corresponding pictures of the printed API doses on each substrate are found in the Appendix.

In Figure 9, plexi was used as substrate and the spacings between the printed dots were measured with the DinoCapture software. The droplets of the higher printed API concentrations (4.78, 58.12 and 118.60 µg/cm^2) had merged together and formed an uneven pattern of larger dots on the surface of the substrate (picture a and b). With the lowest concentration of printed API, 0.59 µg/cm^2, the printed droplets remained completely separated on the surface and the set drop spacing (100 µm) was measured (picture e). An even pattern of vertical and horizontal lines of dots was visible. With printed API concentration of 2.34 µg/cm^2, the printed droplets remained mainly separated (printed dot spacing cohered with set drop spacing, 50 µm), but some merging of droplets was still visible as irregularities in the pattern (picture d).

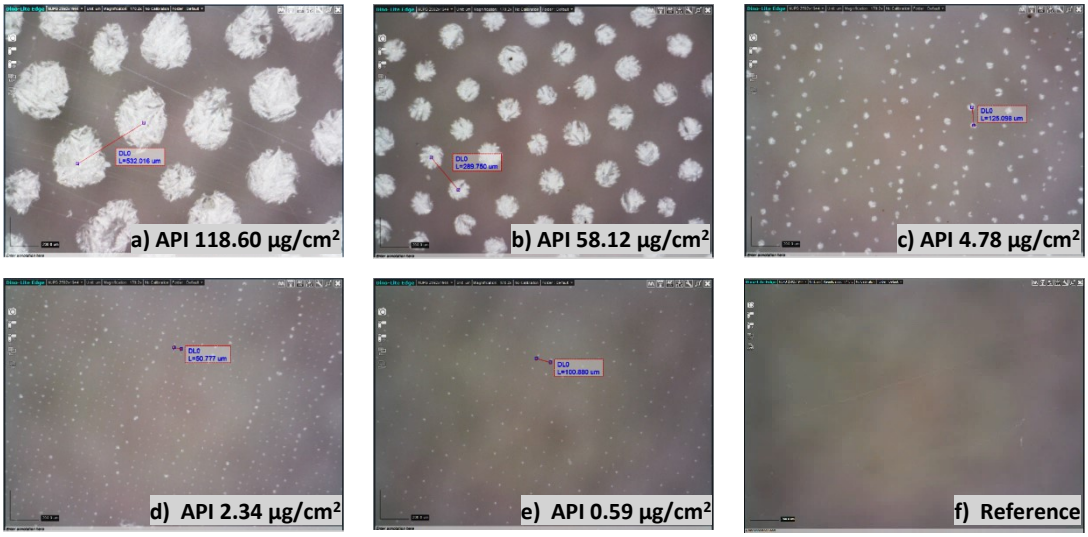

Figure 9. API printed on plexi in five different concentrations. The concentrations were adjusted by changing the drop spacing (method 1). The pictures were taken with the same zoom-setting and the spacing between the printed, dried dots was measured with the software. The dot spacing in picture a) is 532 µm, b) 290 µm, c) 125 µm, d) 50 µm and e) 100 µm.

In Figure 10, blue enamel was used as substrate for printing. The dot-forming behavior of the lower concentrations of printed API, 0.59 and 2.34 µg/cm^2 on enamel, agree with corresponding concentrations printed on plexi (picture d and e). For the lowest printed API

dose, 0.59 µg/cm^2, the droplets remained separated (dot- and set drop spacing 100 µm match) and for an API dose of 2.34 µg/cm^2, some minor merging behavior was observed. However, when printing the three highest doses of API (4.78, 58.12 and 118.60 µg/cm^2), the ink showed a totally different behavior on enamel compared with plexi, and the ink wetted the surface completely. During drying, the highest API dose, 118.60 µg/cm^2, showed some crystallization effect with some larger crystals formed on the surface (picture a). Concentrations of 4.78 and 58.12 µg/cm^2 of printed API, however, dried as an even layer and the theophylline particles were evenly distributed (picture b and c). The same wetting behavior as for enamel appeared for printed glass samples, while printed API-ink on aluminum, steel, epoxy and rubber behaved like on the plexi samples. The behavior can be explained with the surface energies of the substrates and ink-substrate interaction. The high base components of enamel and glass (concluded in Chapter 4.1.3) indicate on alkalic surfaces and by printing a slightly acidic ink on the surface, the liquid wets the surface easily. In other words, the surface energy of the substrate affects the behavior of ink on the surface.

Genia *et al.* and Hirshfield *et al.* found that the recrystallization behavior of a printed API differed depending on the choice of printing substrate and the surface wettability [49] [65]. Hirshfield *et al.* also showed that the crystallization depended on the evaporation rate of the printed sample and the volatility of the carrier fluid [49].

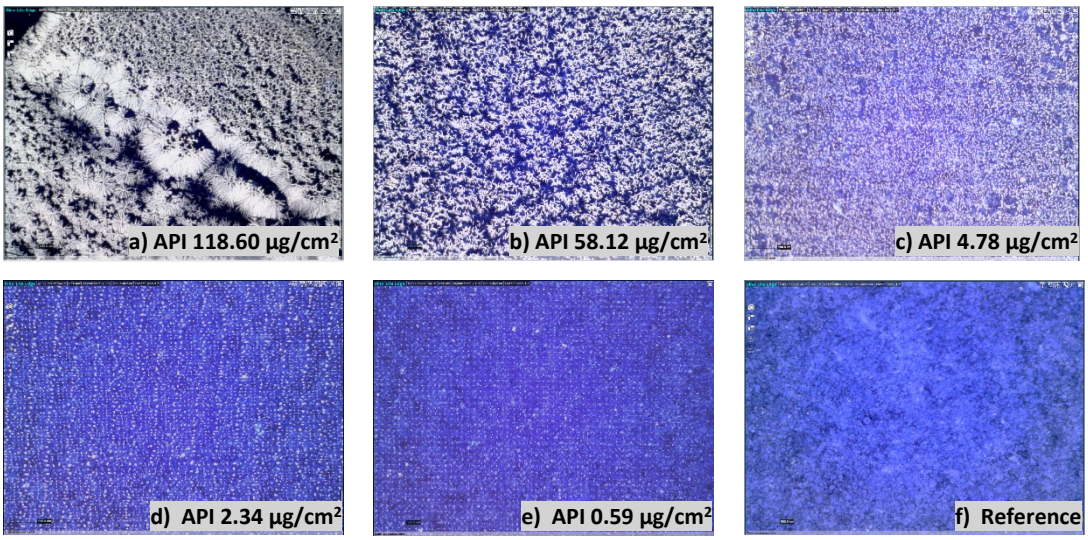

Figure 10. API printed on enamel in five different concentrations. The concentrations were adjusted by changing the drop spacing (method 1). The pictures were taken with the same zoom-setting. The printed, dried API-ink a) undergoes crystallization, b) and c) forms an even pattern of small theophylline crystals, or d) and e) remain in its printed droplets on the surface.

4.2.2 Method 2: Printed API concentration adjusted with ink concentration

By standardizing the drop spacing and adjusting the API concentration in the ink, the corresponding API amounts per area as with method 1 (Chapter 4.2.1) were achieved. In an ideal case, the drop spacing would be set so that the printed droplets remained separated on the surface so that the API would be evenly distributed over the area. For the substrates used in this work, this would mean a drop spacing between 50 and 100 µm. However, the ink formulations were limited to the solubility of theophylline, which did not meet the requirement for the desired API concentrations in the inks. Therefore, a standardized drop spacing of 10 µm was settled and the inks formulated accordingly (see Table 8). Four optimized ink composition with different concentrations of theophylline were printed on three different substrates: aluminum, steel and glass. The fifth ink, 5.80 mg/mL, was already printed with drop spacing 10 with method 1 (Chapter 4.2.1).

Table 8. Listed API concertation in inks. The droplet size was standardized to 10 pL, the drop spacing to 10 µm (1 002 001 droplets per square centimeter) from which the printed API per square centimeter was calculated.

API concentration in ink (mg/mL)	Printed API (µg/cm^2)
0.06	0.59
0.23	2.34
0.48	4.78
5.80	58.12
11.84	118.60

The ink with the highest API concentration, 11.84 mg/mL, clogged the printing nozzle mid-printing and printed only a third of the designed square-pattern (118.60 µg/cm^2). This is assumed to be a result of solvent evaporation at the tip of the nozzle and due to high API loading in the ink. In other words, the 11.84 mg/mL-ink has a shorter latency than the rest of inks. The clogging could most likely have been avoided with automated nozzle-cleaning cycles during the printing process, or by adjusting the non-jetting waveform ("tickle control"). The printed areas were, however, large enough for analysis and the failed printed samples could therefore still be used in this work.

The low API concentration inks, 0.06, 0.23 and 0.48 mg/mL, printed with drop spacing 10 µm, showed coffee staining effect (presented in Chapter 2.1.3) on alumina and steel. In Figure 11, the coffee staining effect is shown on the low API concentration samples, with printed API concentrations of 4.78, 2.34 and 0.59 µg/cm^2 on steel. The printed droplets had merged, and

the solid API accumulated along the outer edges of the dried ink drop (picture c, d and e). Corresponding samples printed on alumina are found in the Appendix. On glass, however, the inks behaved in a totally different way and wetted the surface completely (see Figure 12). The dried API inks formed crystal patterns on the surface. This emphasizes the previously presented results, where it was stated that due to the substrates' high base component, the slightly acidic API-ink behaves differently on glass and enamel than on the rest of the substrates.

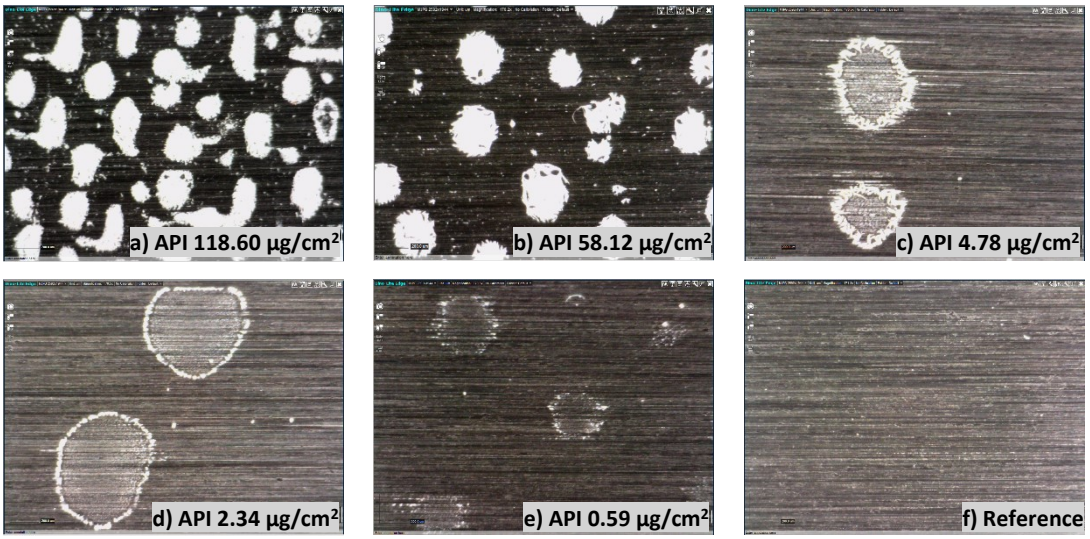

Figure 11. API printed on steel in five different concentrations. The printed concentrations were adjusted by the API concentration in the ink (method 2). The pictures were taken with the same zoom-setting. Coffee staining effect is shown in pictures c), d) and e).

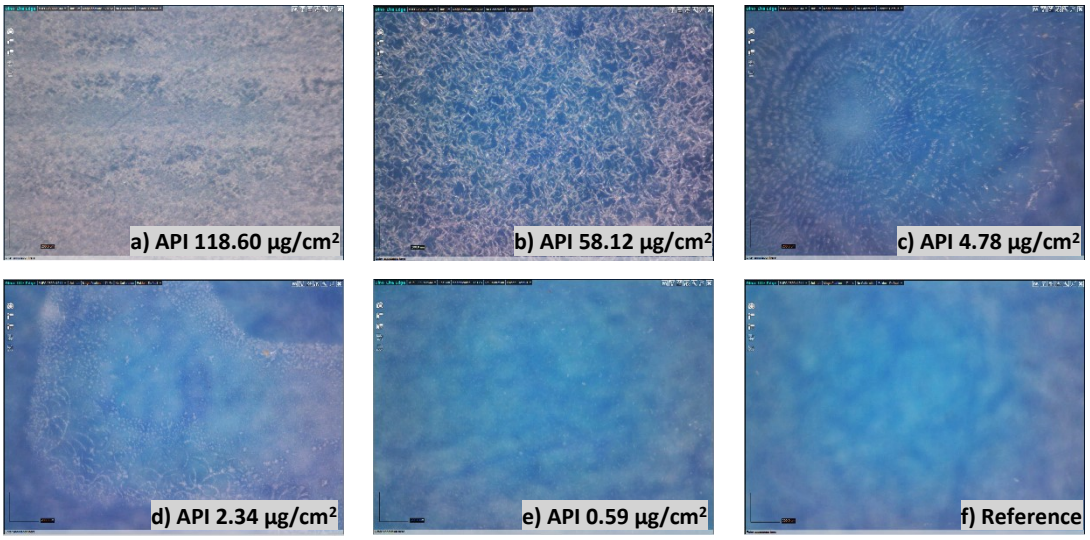

Figure 12. API printed on glass in five different concentrations. The printed concentrations were adjusted by the API concentration in the ink (method 2). The pictures were taken with the same zoom-setting. Theophylline forms crystal pattern on glass when the API-ink is dried.

4.2.3 Method 3: Printed API concentration adjusted with printed layers

Four layers of the optimized ink composition containing 5.8 mg/mL of Theophylline was printed with drop spacing 7 µm on glass sample plates. Each layer contained API 118.60 µg/cm^2 and the layers were dried overnight and analyzed before the next layer was printed on top of the previous one. The single printed layer contained 118.60 µg/cm^2 of printed API, the two layers 237.20 µg/cm^2, the three layers 355.50 µg/cm^2 and the four layers 474.40 µg/cm^2. When a new layer of ink was printed on top of another dried layer of API, the solvents in the ink seemed to redissolve the previously printed API. Figure 13 presents microscopic pictures of the four printed API layers. In the first layer, 118.60 µg/cm^2, the API has dried in somewhat crystalline structures (picture a), while the other API layers have dried quite uniformly. The third layer was printed slightly oblique from the previous layers and the picture shows a distinct line of the layers (picture c). It is, however, concluded that escalating layer-printing of high doses of API, did not affect the appearance of the prints remarkably.

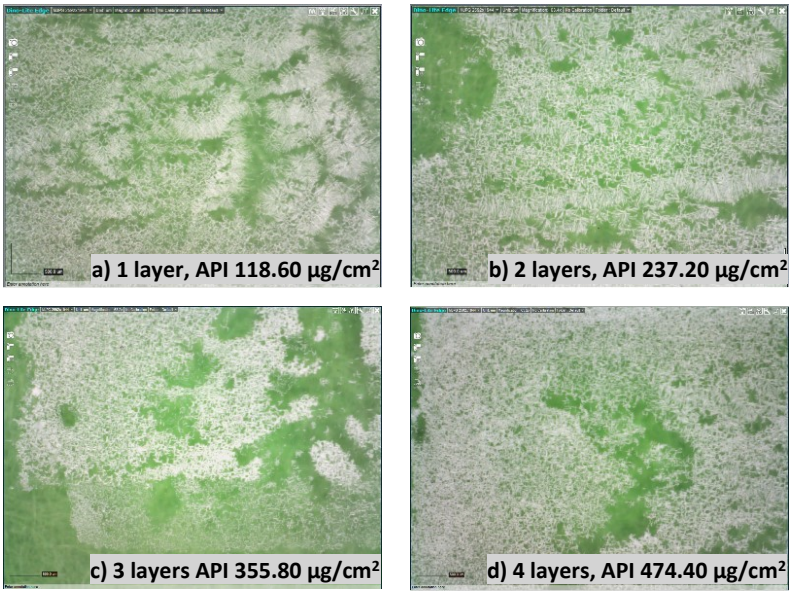

Figure 13. API printed on glass in four different concentrations. The printed API concentrations were adjusted by printing layers of ink on top of one another (method 3) with overnight vacuum dying in between printed layers. The pictures were taken with the same zoom-setting.

4.3 Spectrometric analysis of prints

Three different spectrometric methods were used to analyze the printed API on surfaces, NIR, IR and Raman spectroscopy. The methods were compared and evaluated for detecting small amounts of theophylline on different surfaces. Due to the different ranges of wavelength, the three methods measure different vibrations in the sample molecules. Because of the different active ranges, the methods are considered to be complementary to each other, since e.g. weak IR absorbance often corresponds to a strong Raman emitter. Raman bands are usually sharper than IR, while NIR spectra are rougher. For rapid production analysis, spectrometric methods could be preferred, given that the accuracy and sensitivity are sufficient.

4.3.1 Results from NIR spectroscopy

NIR data was collected from printed paper and plexi samples of five differerent API concentrations per area (concentrations adjusted with drop spacing, method 1) and corresponding placebo samples. Multivariate analysis (principal component analysis, PCA and orthogonal partial least squares, OPLS regression) was made on the data using the SIMCA® 14.1. software (MKS Umetrics, Umeå, Sweden).

In the first steps of building a model, it was already visible that the sample data did not differantiate enough to build a model. This trend displayed for both substrates analyzed. Neighter adjusted light intensity (from 50% to 100%), nor data pre-processing such as standard normalized variate (SNV) and baseline correction improved the modelling. For building a reliable model, the score scatter plot is expected to show significant clustering of the different sampling groups. As seen in Figure 14, the only clustering effect is shown for the two highest printed doses of API, 58.12 and 118.60 ug/cm^2 respectively. The lower doses of API did not differentiate from each other and cluster among the placebo samples. It was concluded that this handheld NIR reflection spectral device was not sensitive enough to detect the lower printed concentrations of API (4.78, 2.34 and 0.59 µg/cm^2).

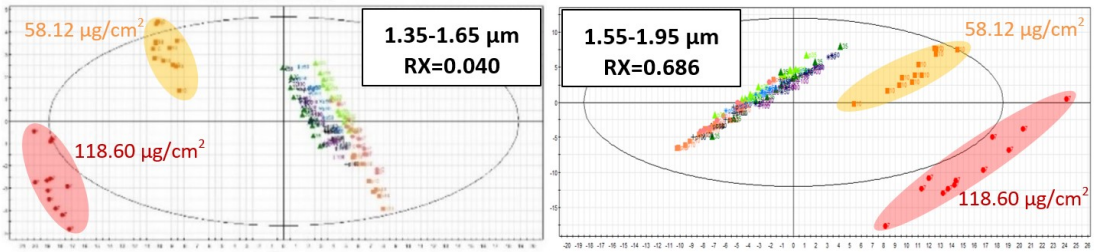

Figure 14. Score scatter plots (1.35-1.65 µm and 1.55-1.95 µm) of OPLS models scaled proportionally to RX of the non-pre-processed data from the plexi-samples. The two highest printed API concentrations (58.12 and 118.60 ug/cm²) show some clustering effect, but the lower printed API concentrations (4.78, 2.34 and 0.59 µg/cm²) were not detected by the instrument and cluster among the placebo-samples.

Vakili *et al.* used the same NIR probes to successfully detect printed levothyroxine and prednisolone on orodispersible films in 2017 [81], but the printed drug concentration was remarkably higher than the lowest concentrations printed in this work (lowest concentration printed with 500 dpi, 80 pL droplets and API concentration of 20 mg/mL in ink, resulting in printed API of about 60 µg/cm^2).

4.3.2 Results from FTIR spectroscopy

The measured IR transmittance spectrum of pure theophylline powder is shown in Figure 15. The powder was dried in a vacuum oven (80 Torr, 60°C) overnight before measurements to remove excess water. The spectrum matches the reference spectra of anhydrous theophylline, found in the literature with tallest peak at 1660 cm^{-1} [85].

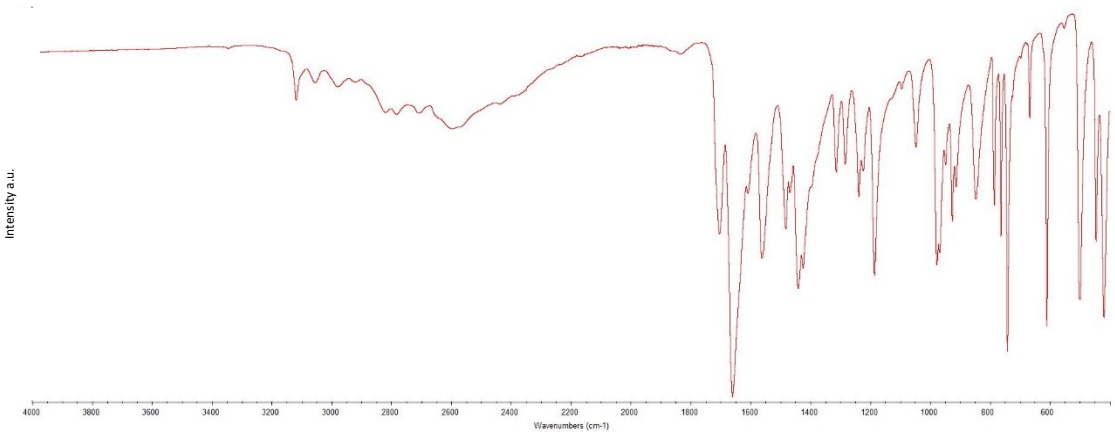

Figure 15. Measured IR transmittance spectrum of theophylline powder.

Samples printed in five different concentrations on rubber and aluminum are shown in Figure 16 and Figure 17 respectively. The theophylline concentration per area was adjusted with drop spacing (method 1) and the samples were dried in vacuum overnight before measurements. Corresponding IR spectra of other substrates (steel, plexi, epoxy, enamel, glass and paper) are found in Appendix. The spectra show peaks in the significant ranges for theophylline, especially in the 1600-1700 cm^{-1} and 500 cm^{-1} regions. A trend where higher API printed concentration correlates to bigger peaks was observed for respective substrate. Depending on the substrate, the lowest concentrations of printed theophylline did not differ sufficiently from the reference spectrum. The API amount was, however, concluded to be extremely small and might reach the limit of detection for the instrument. Printed theophylline was best shown with IR on aluminum and steel (detected API doses as low as 0.59-2.34 µg/cm^2) and least shown on paper and rubber (detected API doses as low as 4.78-58.12 µg/cm^2).

Samples printed with placebo ink in different concentrations (corresponding to the API doses adjusted with drop spacing, method 1) match the substrate's reference spectrum for all substrates, regardless of printed ink amount (see Appendix). This was rather predictable, since the ink solvents were expected to evaporate during vacuum oven drying overnight. Furthermore, it is concluded that the increasing peaks for the API-samples is due to increasing amount of printed theophylline and not increasing amount of printed ink solution.

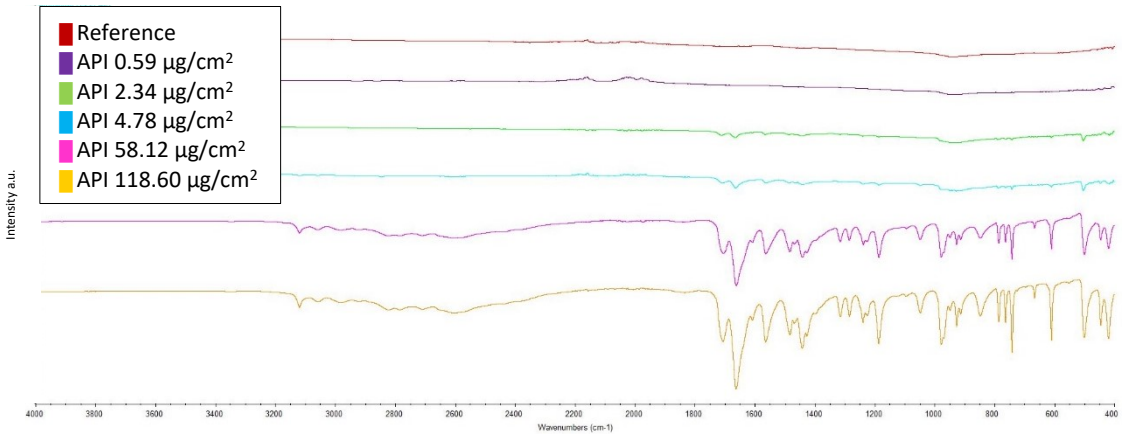

Figure 16. Transmittance IR spectra of theophylline printed on aluminum in five different concentrations. The concentrations were adjusted by changing the drop spacing (method 1). Reference spectrum of the plain substrate was also measured. The spectra show peaks in the significant ranges for theophylline.

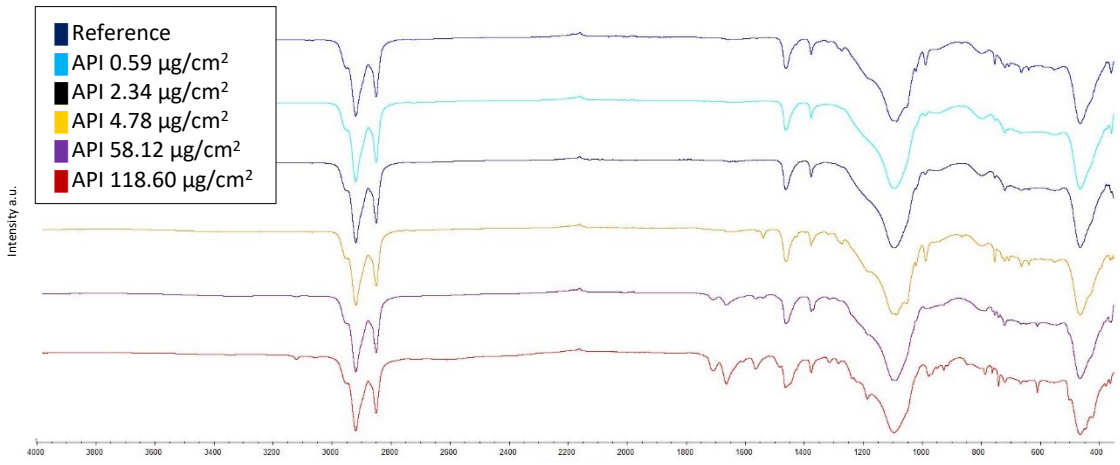

Figure 17. Transmittance IR spectra of theophylline printed on rubber in five different concentrations. The concentrations were adjusted by changing the drop spacing (method 1). Reference spectrum of the plain substrate was also measured.

IR spectra of samples printed with method 2, by keeping the drop spacing at 10 µm and adjusting the API concentration in the ink, are shown in Figure 18 for aluminum samples. Corresponding IR spectra of steel and glass samples are found in the Appendix. The samples were dried in a vacuum oven overnight before measurements. The same trend as for samples printed with method 1 was noticed for these samples: higher printed API concentration correlates to bigger peaks for respective substrate and the lower printed API concentrations were not visible.

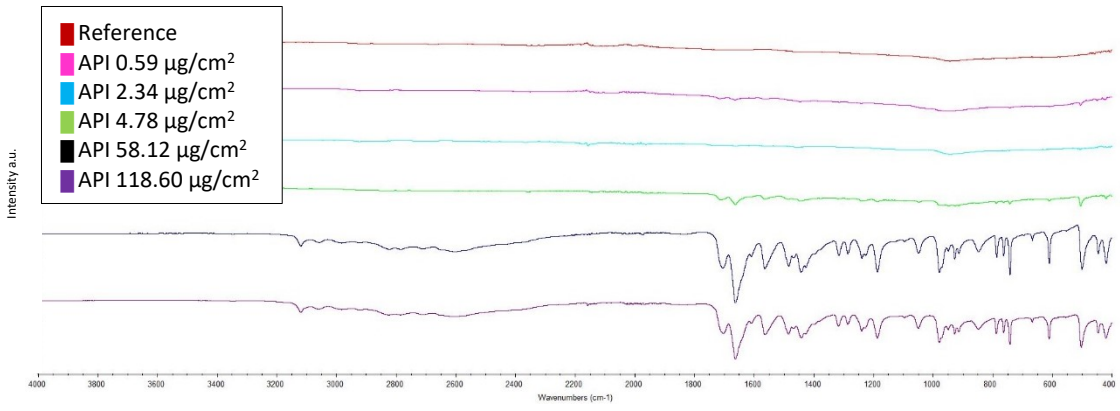

Figure 18. Transmittance IR spectra of theophylline printed on aluminum in five different concentrations. The printed concentrations were adjusted by the API concentration in the ink (method 2). Reference spectrum of the plain substrate was also measured.

In Figure 19, IR spectra of glass samples printed with method 1 and 2 were compared to each other. The printed API concentration is either achieved by adjusting the drops spacing (method 1) or API concentration in the ink (method 2). According to Figure 19, samples printed with method 2 have more significant IR peaks than the samples printed with method 1. However, by comparing Figure 16 to Figure 17, aluminum samples printed with method 1 have some small IR peaks even at lower concentration (2.34 µg/cm^2), while corresponding sample printed with method 2 did not show any IR peaks. This could be a result of the inhomogeneous printed area due to merging of droplets and that only one analysis was done per sample. An alternative for circumvention is repeated analyses from several different spots of the samples.

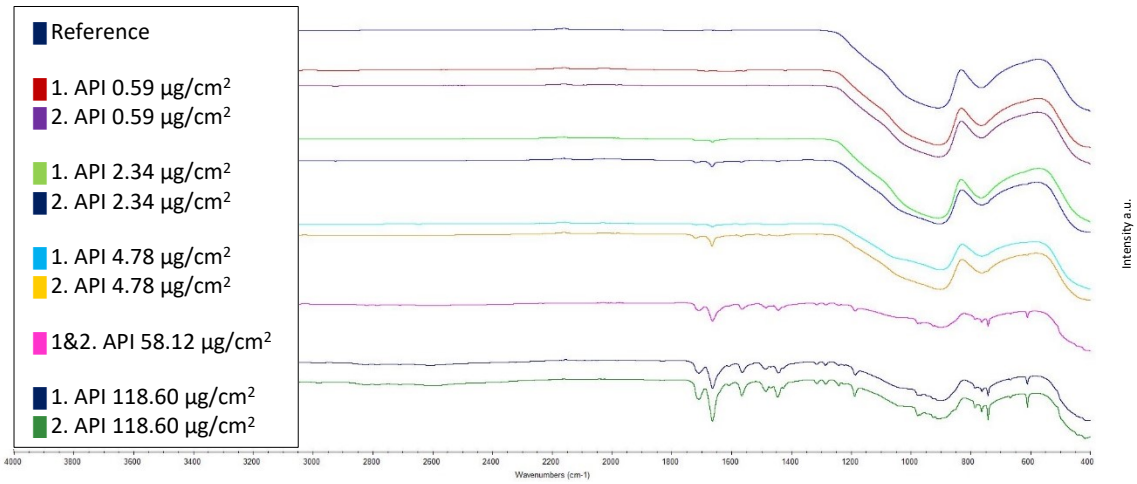

Figure 19. Transmittance IR spectra of theophylline printed on glass in five different concentrations with two methods for distributing API. The printed concentrations were adjusted by either 1. changing the drop spacing (method 1) or by 2. adjusting the API concentration in the ink (method 2). Reference spectrum of the plain substrate was also measured.

The printed API concentration was drastically increasing by printing several layers of API on top of one another (method 3). Glass was used as substrate and each layer was dried overnight and analyzed before the next layer was printed on top of the previous one. The IR spectra (Figure 20) did not show a significant difference between the printed layers (printed API concentration 118.60, 237.20, 355.50 and 474.40 µg/cm^2). The printed API per area is yet proportionally high for all printed layers and the API covers the surface almost completely for all printed concentrations (see Figure 13).

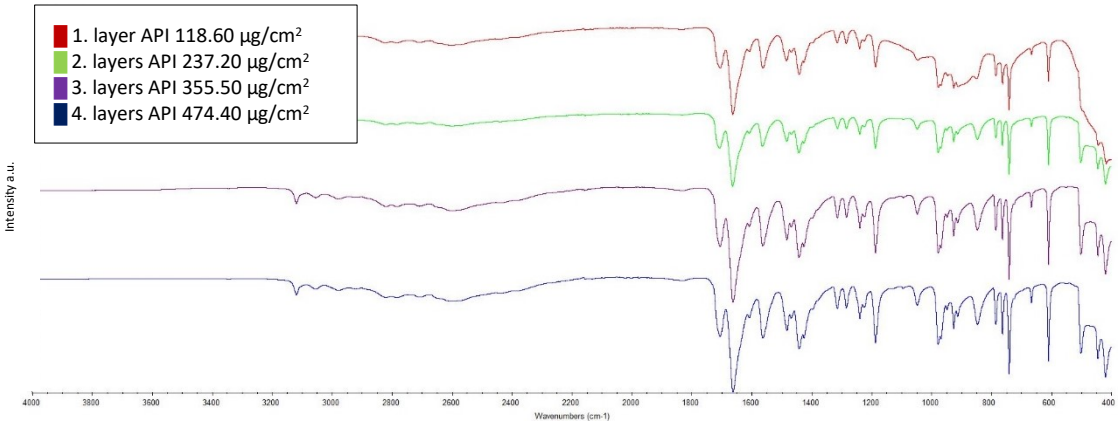

Figure 20. Transmittance IR spectra of theophylline printed on glass in four different concentrations. The printed API concentrations were adjusted by printing layers of ink on top of one another (method 3) with overnight vacuum dying in between printed layers.

4.3.3 Results from Raman spectroscopy

Raman absorbance spectra of the pure theophylline powder (Figure 21) matched reference spectra from the literature [78]. However, the glass sample, printed with escalating doses of API by printing several layers on top of one another (method 3), did not show any Raman absorbance peaks whatsoever (see Figure 21). Different instrument power settings were tested (0.05-0.5 W). The results were surprisingly unsatisfactory, since the printed API concentrations were proportionally high (118.60, 237.20, 355.50 and 474.40 µg/cm2), compared to samples printed with method 1 and 2 and detected with FTIR.

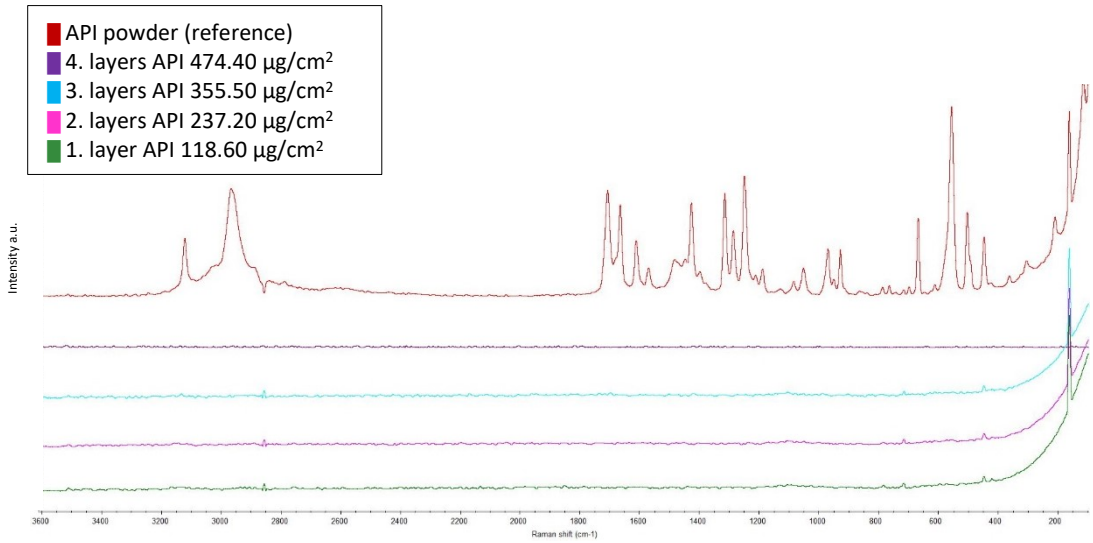

Figure 21. Raman absorbance spectra of theophylline powder and printed in four different concentrations on glass by printing layers on top of one another (method 3) with overnight vacuum dying in between printed layers.

5 CONCLUSIONS

When printing pharmaceuticals, the intention of the final product is of great importance in aspect to accuracy, consistency, ink-substrate adhesion and stability of both ink and the final product. The investigation of this thesis was focused on applying small amounts (µg) of API on different materials used in drug production facilities, and therefore differs notably from the majority of previously done studies, which often focus on printing APIs on different porous substrates, intended to be consumed. In those cases, factors like bioavailability and toxicity need to be taken into consideration in a whole other way than in this work, where the printed product is intended to eventually be used for cleaning validation purposes. Compared to the majority of previously done studies on printing of APIs, this work faces new challenges and gives a wider perspective on inkjet printing of APIs.

The most important factor for a successful print is the API-containing ink formulation and its applicability for the printer. The physicochemical properties of a printable ink must lie within a narrow window in aspect to surface tension, viscosity, density and the API's solubility or stability as colloidal particles of suitable sizes in the ink liquid is crucial. An ink solution consisting of glycerol, ethanol and water as carrier fluids in ratio 10:45:45 was concluded to be suitable for printing theophylline with Dimatix DMP 2830 material printer (10 pL droplet cartridges) with a preset "caffeine" waveform and 13-15 V piezoelectric droplet firing.

The optimal theophylline loading in the ink was concluded to be 5.8 mg/mL, but other ink-concentrations were also printed, but with less successful printing results. Lower theophylline-loaded inks (0.06, 0.23, 0.48 mg/mL) tended to show a coffee staining effect when printed and dried on a surface. This was concluded to be a result of API-particle accumulation among the outer edges of the ink droplet, while the ink-solvents evaporated. An ink loaded with theophylline 11.84 mg/mL, clogged the nozzle mid printing due to high API-loading and solvent evaporation at the nozzle. However, the ink was yet printable, and the nozzle clogging could most probably be avoided by adjusting the jetting and non-jetting waveform and/or add automated nozzle cleaning, maintenance cycles. Another way of achieving high API-loaded inks, limited by the solubility of the API, would have been adjusting the ink solvents. Acetone and dimethyl sulfoxide (DMSO) are known for dissolving poorly soluble APIs and have previously been used in various printings. Nanosuspensions and nanoemulsions of APIs could also be used to increase the loading of poorly soluble APIs in carrier fluids. The ink-printer and ink-substrate combability is yet needed to be taken into

consideration, as well as the previously mentioned physicochemical properties for a printable ink. Another perspective is printhead design development. Today, a lot of research is focused on development of printable API-containing fluids and applying it to already existing printing technology. But by taking printhead design and underlying technology into consideration when developing printed pharmaceuticals, the opportunities widen remarkably. [3]

Different amounts of theophylline were successfully printed on all of the eight different substrates investigated. The printed theophylline-ink behaved different on the surfaces of the different substrates. Paper was used as reference substate and the porous structure absorbed ink, while the other substrates, steel, aluminum, glass, plexi, enamel, epoxy and rubber, were non-porous and the ink remained and dried on the surface. It was concluded that the surface properties such as dispersive, polar, acid and base components of surface energy, as well as the surface roughness, determined the ink-substate behavior. According to the choice of substrate and how closely the ink droplets were printed, the droplets remained separated on the surface or merged into bigger units or wetted the surface entirely (only on glass and enamel).

The fundamental part for being able to utilize printed APIs for cleaning validation purposes, is the printed amount of API per area. In this work, three methods were used for adjusting the theophylline amount per area and one showed more potential than the others. The optimized ink composition containing 5.8 mg/mL theophylline was successfully printed on all substrates in five different concentrations per area (0.59, 2.34, 4.78, 58.12, 118.60 µg/cm^2) by adjusting the drop spacing. This was presented to be the most suitable method for adjusting the printed API concentration per area for this work. The printed theophylline dose per area was also increased drastically by printing several layers of ink with the highest API dose, 118.60 µg/cm^2, on each other. Since the layers where dried in a vacuum oven over night, before the next layer was printed on top of the previous one, this method was rather time consuming and could only be recommended for printing high doses of API per area, when the maximum API loading in the ink, limited to the solubility of the API, is exceeded.

Of the three spectrometric methods used for analyzing the printed samples, FTIR-ATR is concluded to be the most sensitive of them. The handheld two-piece NIR device did not seem to be sensitive enough to detect the lower doses of printed API and in the first crucial steps of PCA multivariate analyses, only printed API doses higher than 58.12 µg/cm^2 were detected. This device could possibly be suitable for in- or on-line measurements, or for detecting higher

doses of API in drug production facilities with higher MAC, but not necessarily for the strictest MACs. It is yet found that the NIR-device is rather old (> 10 years) and that newer devices with better technology are already available on the market. It is suggested that more research is done on newer handheld NIR-devices, to scope the potential for NIR as a sensitive and reliable method for detecting small amounts of APIs on surfaces.

While the pure theophylline powder was detected with Raman spectroscopy (1064 nm laser), none of the printed samples (highest API dose 474.40 µg/cm^2) showed any Raman signal whatsoever. The results were surprisingly unsatisfactory since Raman is commonly known for being a rather sensitive analytical method. An option would have been to analyze the samples with other Raman wavelengths (another laser) and thereafter determine the sensitivity for Raman.

Theophylline concentrations as low as 2.34 µg/cm^2 were detected with a stationary FTIR-ATR on aluminum, steel, glass and plexi. The IR-peaks were quite weak, but still noticeable for the lower concentrations of printed API, while the higher printed API concentrations (58.12, µg/cm^2 and higher) showed clear theophylline peaks with FTIR spectroscopy on all investigated substrates. It is yet concluded that the surface of printed API was inhomogeneous and that the API did not spread evenly on the surface due to merging of droplets. Repetitive analysis would be needed to get a representative result of a printed sample area. However, the investigation showed promising results for spectrometric methods for detecting small amounts API on different surfaces. Several handheld spectrometric instruments are already available on the market and depending on the reliability and sensitivity of the handheld instruments, these could potentially be used parallel or even replace currently used HPLC analysis.

It is determined that inkjet printing is an effective way to dispense small doses of APIs on different surfaces and shows potential for generating precise calibration standards. Escalating doses are proven to be detected both visually and by FTIR-ATR spectroscopy. Needless to say, that more research and pharmaceutical method validation would be needed to justify printing as an accurate and reliable method for prototyping drug residuals in production facilities and pipelines. More research with printing of different APIs, dilution series and analytical sampling would be needed to successfully do a multivariate analysis. However, printing as technology shows great potential for the pharmaceutical industry in aspect to analytical instrument development and calibration.

6 SWEDISH SUMMARY

6.1 Tryckning och spektrometrisk detektering av aktiva farmaceutiska substanser på olika ytor

Bläckstråletryckning anses vara en exakt och relativt snabb metod för noggrann dosering av material. I och med flexibla möjligheter för mönster och dosering har tekniken visat potential för medicinsk teknologi, biomedicin och läkemedelsindustrin i form av personligt framställda medicinska produkter. Mycket forskning görs inom området och de första bläckstråletryckta medicinska produkterna finns redan på marknaden. Förutom framställning av produkter ämnade att konsumeras, har bläckstråletryckning även potential att utnyttjas inom andra områden i läkemedelsindustrin som t.ex. för att modellera läkemedelsrester i produktionsanläggningar. Tryckta modeller för läkemedelsrester kunde användas för att kalibrera både redan etablerade analysinstrument för renlighetsvalideringar och i utvecklingen av nya analysinstrument. Med hjälp av bläckstråletryckning modelleras i den här avhandlingen läkemedel på olika material, ofta förekommande i produktionsanläggningar för läkemedel. Fokus för arbetet var att framställa ett tryckbart bläck som innehåller läkemedel (teofyllin), trycka bläcket på åtta olika material i olika koncentrationer per area (0,59-474,4 μg/cm^2) och undersöka de tryckta proverna med tre olika spektroskopiska metoder: IR, NIR och Raman.

Den första utmaningen för att trycka ett läkemedel är att framställa ett bläck med rätt tryckningsegenskaper för ifrågavarande tryckmetod. De tre mest betydelsefulla fysikalisk-kemiska bläckegenskaperna för bläckstråletryckning är ytspänning, viskositet och partikelstorlek. Ett läkemedel kan antingen bilda en kolloidal dispersion och/eller vara upplöst i bläcklösningen. Läkemedlets löslighet och/eller storleken på de kolloidala partiklarna är begränsande faktorer för framställningen av ett tryckbart bläck. Både bläckets ytspänning och viskositet har inverkan på hur en droppe formas i munstyckets öppning, avlossas och beter sig på substratets yta. Bläckegenskaperna kan justeras med att variera sammansättningen på transportvätskan med lösningsmedel och tillsatsämnen. I arbetet framställdes flera sammansättningar av bläck som innehöll teofyllin och bläckens fysikalisk-kemiska egenskaper undersöktes. Slutsatsen av laborationerna var att ett bläck bestående av glycerol, etanol och vatten i förhållande 10 %, 45 % och 45 %, och med olika koncentrationer av teofyllin mellan 0,06 - 12 mg/mL, fungerade för bläckstråletryckning.

I avhandlingen användes en bläckstråletryckare med Drop-on-Demand-piezoelektrisk dosering. Bläckkassetterna, med ett teofyllin-bläck sattes fast på ett rörligt skrivhuvud som rörde sig över substratet och skrev ut ett förinställt mönster med hjälp av 10 pL:s droppar. Det tryckta mönstret var kvadratiska rutor med sidlängden 1 cm och de tryckta proverna torkades i vacuumugn över natten för att evaporera bläckets lösningsmedel innan analyserna. Den tryckta koncentrationen teofyllin per area varierades med tre olika metoder, nämligen 1) genom att använda ett bläck med teofyllin i koncentrationen 5,8 mg/mL och variera avståndet mellan de tryckta dropparna (7, 10, 35, 50 och 100 µm) 2) genom att standardisera droppavståndet till 10 µm och variera teofyllinkoncentrationen i bläcket (0,06, 0,23, 0,48, 5,80, 11,84 mg/mL) 3) genom att trycka flera lager av bläck på varandra (droppavstånd 7 µm och teofyllinkoncentration 5,8 mg/mL). Metod 1 konstaterades dock lämpa sig bäst för det här arbetes ändamål.

Åtta olika material användes som substrat för tryckningarna: aluminium, stål, epoxi, glas, plexi, emalj, gummi och papper. De sju förstnämnda är material som ofta förekommer i produktionsanläggningar för framställning av läkemedel och papper användes som referensmaterial för tryckningarna. På grund av substratens varierande ytenergier, vätte det tryckta bläcket ytorna olika. Papper var poröst och absorberade bläcket medan resten av substraten var oporösa och nära tryckta bläckdroppar slogs i vissa fall samman till större droppar som ett resultat av vätning, ytspänning och lagen om minimerad ytenergi. Vid torkning evaporerade lösningsmedlen i bläcket och teofyllin kvarlämnades som punkter eller kristallenheter på substratets yta. Det konstaterades att på grund av teofyllinets sura pH, vätte bläcket ytor med hög baskomponent, glas och emalj, fullständigt.

För NIR-analyser användes ett handhållet instrument med analysområde 1350-1950 nm och för IR- samt Ramananalyserna användes en spektrometer. IR-analyser gjordes med FTIR-ATR (400-4000 cm^{-1}) och Raman med 1064 nm laser (100-3600 cm^{-1}). Det visade sig att varken NIR- eller Ramaninstrumenten var tillräckligt känsliga för att analysera de små mängderna tryckt teofyllin på de olika substraten. I IR-analyserna däremot, framträdde de signifikanta topparna för teofyllin i spektra för samtliga koncentrationer av tryckt teofyllin. Dock var topparna för de lägsta koncentrationerna av teofyllin ytterst små på grund av de låga halterna läkemedel per area (0,59 och 2,34 µg/cm^2). Förutom de tryckta proverna med eskalerande doser av teofyllin, trycktes även parallella prover med ett placebo-bläck (utan läkemedel) för att garantera att analyserna indikerade på ökad mängd teofyllin, och inte ökad mängd bläcklösning. Som förväntat evaporerade allt tryckt placebo-bläck från ytorna och samtliga

placebo-provers IR-spektra motsvarade substratens referensspektrum. Det kan alltså konstateras att en ökad dos tryckt teofyllin ger större utslag (toppar) i IR-spektra på samtliga substrat.

Tryckning av aktiva farmaceutiska substanser konstateras vara ett effektivt sätt att dosera små mängder läkemedel på olika ytor och påvisar stor potential för att framställa standarder för renlighetsvalideringar i läkemedelsindustrin. Tryckta standarder kunde användas för kalibrering av redan etablerede analysmetoder för renlighetsvalideringar och i utvecklingen av nya analysinstrument.

REFERENCES

[1] M. Maniruzzaman (Ed.), T. G. West and T. J. Bradbury, "3D Printing: A Case of ZipDose® Technology – World's First 3D Printing Platform to Obtain FDA Approval for a Pharmaceutical Product," in *3D and 4D Printing in Biomedical Applications: Process Engineering and Additive Manufacturing*, John Wiley & Sons, 2019, pp. 53-80.

[2] S. Beg, W. H. Almalki, A. Malik, M. Farhan, M. Aatif, Z. Rahman, N. K. Alruwaili, M. Alrobaian, M. Tarique and M. Rahman, "3D printing for drug delivery and biomedical applications," *Drug Discovery Today,* vol. 25, no. 9, pp. 1668-1681, 2020.

[3] R. Daly, T. S. Harrington, G. D. Martin and I. M. Hutchings, "Inkjet printing for pharmaceutics – A review of research and manufacturing," *International Journal of Pharmaceutics,* vol. 494, no. 2, pp. 554-567, 2015.

[4] "Orion Group Financial Statement Release 2020," Orion Corporation, 2020.

[5] M. S. Arayne, N. Sultana and M. K. Zaman, "Historical incidents leading to the evolution of good manufacturing practice," *Accreditation and Quality Assurance,* vol. 13, no. 8, pp. 431-432, 2008.

[6] E. Rivera and P. Lopolito, "Evaluating Surface Cleanliness Using a Risk-Based Approach," *Pharmaceutical Technology,* vol. 41, no. 12, pp. 28-37, 2017.

[7] S. Magdassi, The chemistry of inkjet inks, Singapore: World Scientific Publishing Company, 2010.

[8] I. M. Hutchings and G. D. Martin, Inkjet Technology for Digital Fabrication, XXXX: John Wiley & Sons, Ltd, 2013.

[9] H. Wickström, Exploring Printed Drug Formulations for Inkjet and Stencil Printing, Åbo, Finland : Ghent, Belgium : Ghent University: Åbo Akademi University, 2020.

[10] H. P. Le, "Progress and Trends in Ink-jet Printing Technology," *Journal of Imaging Science and Technology,* pp. 49-62, 1998.

[11] B. Derby, "Inkjet Printing of Functional and Structural Materials: Fluid Property Requirements, Feature Stability, and Resolution," *Annual Review of Materials Research,* vol. 40, pp. 395-414, 2010.

[12] D. Jang, D. Kim and J. Moon, "Influence of Fluid Physical Properties on Ink-Jet Printability," *Langmuir,* pp. 2629-2635, 2009.

[13] S. Azizi Machekposhti, S. Mohaved and R. J. Narayan, "Inkjet dispensing technologies: recent advances for novel drug discovery," *Expert Opinion on Drug,* vol. 14, no. 2, pp. 101-113, 2019.

[14] S. Yamaguchi, A. Uneo, Y. Akiyama and K. Morishima, "Piezoelectric inkjet-based single-cells printing by image processing for high efficiency and automatic cell printing," in *17th International Conference on Miniaturized Systems for Chemistry and Life Sciences*, Freiburg, Germany, 2013.

[15] I. FUJIFILM Dimatix, "ManualsLib," 26 March 2008. [Online]. Available: www.manualslib.com/manual/1238531/Dimatix-Dmp-2800-Series.html. [Accessed 12 January 2021].

[16] S. Kamisuki, T. Hagata, C. Tezuka, Y. Nose, M. Fujii and M. Atobe, "A low power, small, electrostatically-driven commercial inkjet head," in *IEEE International Conference on Micro Electro Mechanical Systems*, Heidelberg, Germany, 1998.

[17] E. Elele, Y. Shen, R. Susarla, B. Khusid, G. Keyvan and B. Michniak-Kohn, "Electrodeless electrohydrodynamic drop-on-demand encapsulation of drugs into porous polymer films for fabrication of personalized dosage units," *Journal of Pharmaceutical Sciences,* pp. 2523-2533, 2012.

[18] H. Gudapati, M. Dey and I. Ozbolat, "A comprehensive review on droplet-based bioprinting: Past, present and future," *Biomaterials.,* pp. 20-42, 2016.

[19] J. F. Dijksman, "Hydrodynamics of Small Tubular Pumps," *Journal of Fluid Mechanics,* vol. 139, pp. 173-191, 1984.

[20] J. E. Fromm, "Numerical Calculation of the Fluid Dynamics of Drop-on-Demand Jets," *IBM Journal of Research and Development,* vol. 28, no. 3, pp. 322-333, 1984.

[21] M. Döring, "Ink-jet printing," *Philips Technical Review,* vol. 40, no. 7, pp. 192-198, 1982.

[22] S. Lee, G. A. Webster, J. R. Pietrzyk and F. Barmaki, "Inks having high molecular weight polysaccharides". United States Patent US6790268B2, 14 9 2004.

[23] "EPSON," Epson America, Inc., 2021. [Online]. Available: www.epson.com. [Accessed 23 3 2021].

[24] B. R. Bird, W. E. Stewart and E. N. Lightfoot, Transport Phenomena (2nd ed), John Wiley & Sons, Inc., 2002.

[25] J. Madejski, "Droplets on impact with a solid surface," *International Journal of Heat and Mass Transfer,* vol. 26, no. 7, pp. 1095-1098, 1983.

[26] B. He, N. A. Patankar and J. Lee, "Multiple Equilibrium Droplet Shapes and Design Criterion for Rough Hydrophobic Surfaces," *Langmuir,* vol. 19, no. 13, pp. 4999-5003, 2003.

[27] M. E. R. Shanahan and C. Bourgès, "Effects of evaporation on contact angles on polymer surfaces," *International Journal of Adhesion and Adhesives,* vol. 14, no. 3, pp. 201-205, 1994.

[28] J. F. Dijksman and A. Pierika, "Fluid dynamical analysis of the distribution of ink jet printed biomolecules in microarray substrates for genotyping applications," *Biomicrofluidics,* vol. 2, no. 044101, 2008.

[29] R. D. Deegan, O. Bakajin, T. F. Dupont, G. Huber, S. R. Nagel and T. A. Witten, "Contact line deposits in an evaporating drop," *Physical Review E,* vol. 62, no. 1, pp. 756-765, 2000.

[30] R. Deegan, O. Bakajin, T. Dupont, G. Huber, S. R. Nagel and T. A. Witten, "Capillary flow as the cause of ring stains from dried liquid drops," *Nature,* vol. 389, pp. 827-829, 1997.

[31] C. Voura, N. Schroedl, M. M. Gruber, D. Strohmeier, B. Eitzinger, W. Bauer, G. Brenn, J. G. Khinast and A. Zimmer, "Printable medicines: A microdosing device for producing personalised medicines," *Pharmaceutical Technology Europe,* vol. 23, no. 1, pp. 32-36, 2011.

[32] B. M. Wu, S. W. Borland, R. A. Giordano, L. G. Cima, E. M. Sachs and M. J. Cima, "Solid free-form fabrication of drug delivery devices," *Journal of Controlled Release,* vol. 40, no. 1-2, pp. 77-87, 1996.

[33] I. Ursan, L. Chiu and A. Pierce, "Three-dimensional drug printing: A structured review," *Journal of the American Pharmacists Association,* vol. 53, no. 2, pp. 136-144, 2013.

[34] S. Khaled, J. Burley, M. Alexander and C. Roberts, "Desktop 3D printing of controlled release pharmaceutical bilayer tablets," *International Journal of Pharmaceutics,* vol. 461, no. 1-2, pp. 105-111, 2014.

[35] R. G. Strickley, "Solubilizing excipients in oral and injectable formulations.," *Pharmaceutical Research,* vol. 21, p. 201–230, 2004.

[36] A. J. Radcliffe, J. L. Hilden, Z. K. Nagy and G. V. Reklaitis, "Dropwise Additive Manufacturing of Pharmaceutical Products Using Particle Suspensions," *Journal of Pharmaceutical Sciences,* vol. 108, no. 2, pp. 914-928, 2019.

[37] N. Sandler, A. Määttänen, P. Ihalainen, L. Kronberg, A. Meierjohann, T. Viitala and J. Peltonen, "Inkjet printing of drug substances and use of porous substrates-towards individualized dosing," *Journal of Pharmaceutical Sciences,* vol. 100, no. 8, pp. 3386-3395, 2011.

[38] N. Genina, D. Fors, M. Palo, J. Peltonen and N. Sandler, "Behavior of printable formulations of loperamide and caffeine on different substrates--effect of print density in inkjet printing," *International Journal of Pharmaceutics,* 2013.

[39] C. Varan, H. Wickström, N. Sandler, Y. Aktaş and E. Bilensoy, "Inkjet printing of antiviral PCL nanoparticles and anticancer cyclodextrin inclusion complexes on bioadhesive film for cervical administration," *International Journal of Pharmaceutics,* vol. 531, no. 2, pp. 701-713, 2017.

[40] A. B. M. Buanz, C. C. Belaunde, N. Soutari, C. Tuleu, M. O. Gul and S. Gaisford, "Ink-jet printing versus solvent casting to prepare oral films: Effect on mechanical properties and physical stability," *International Journal of Pharmaceutics,* vol. 494, no. 2, pp. 611-618, 2015.

[41] G. K. Eleftheriadis, P. K. Monou, N. Bouropoulos and D. G. Fatouros, "In Vitro Evaluation of 2D-Printed Edible Films for the Buccal Delivery of Diclofenac Sodium," *Materials,* vol. 11, no. 5, p. 864, 2018.

[42] Y. Thabet, D. Lunter and J. Breitkreutz, "Continuous inkjet printing of enalapril maleate onto orodispersible film formulations," *International Journal of Pharmaceutics,* vol. 546, no. 1-2, pp. 180-187, 2018.

[43] M. Kyobula, A. Adedeji, M. R. Alexander, E. Saleh, R. Wildman, I. Ashcroft, P. R. Gellert and C. J. Roberts, "3D inkjet printing of tablets exploiting bespoke complex geometries for controlled and tuneable drug release," *Journal of Controlled Release,* pp. 207-215, 2017.

[44] J. Pardeike, D. M. Strohmeier, N. Schrödl, C. Voura, M. Gruber, J. G. Khinast and A. Zimmer, "Nanosuspensions as advanced printing ink for accurate dosing of poorly soluble drugs in personalized medicines," *International Journal of Pharmaceutics,* vol. 420, no. 1, pp. 93-100, 2011.

[45] G. Kollamaram, A. Faucher, D. M. Croker and G. M. Walker, "Valvejet Technology for the Production of a Personalised Fixed Dose Combination of Ramipril and Glimepiride: an Investigative Study on the Stability of Ramipril," *Pharmaceutical Research,* vol. 39, no. 9, p. 181, 2018.

[46] M. Edinger, D. Bar-Shalom, J. Rantanen and N. Genina, "Visualization and Non-Destructive Quantification of Inkjet-Printed Pharmaceuticals on Different Substrates Using Raman Spectroscopy and Raman Chemical Imaging," *Pharmaceutical Research,* pp. 1023-1036, 2017.

[47] R. P. E. Montenegro-Nicolini M, M. O. Jara, P. R. Vuddanda, A. Neira-Carrillo, N. Butto, S. Velaga and J. O. Morales, "The Effect of Inkjet Printing over Polymeric Films as

Potential Buccal Biologics Delivery Systems," *AAPS PharmSciTech,* vol. 19, pp. 3376-5587, 2018.

[48] H.-Y. Hsu, S. J. Toth, G. J. Simpson, L. S. Taylor and M. T. Harris, "Effect of Substrates on Naproxen-Polyvinylpyrrolidone Solid Dispersions Formed via the Drop Printing Technique," *Journal of Pharmaceutical Sciences,* vol. 102, no. 2, pp. 638-648, 2013.

[49] L. Hirshfield, A. Giridhar, L. Taylor, M. Harris and G. Reklaitis, "Dropwise Additive Manufacturing of Pharmaceutical Products for Solvent-Based Dosage Forms," *Journal of Pharmaceutical Sciences,* vol. 103, no. 2, pp. 496-506, 2014.

[50] H.-Y. Hsu, M. T. Harris, S. J. Toth and G. J. Simpson, "Drop printing of pharmaceuticals: Effect of molecular weight on PEG coated-naproxen/PEG 3350 solid dispersions," *AIChE Journal,* vol. 61, no. 12, pp. 4502-4508, 2015.

[51] E. Içten, A. Giridhar, L. S. Taylor, Z. K. Nagy and G. V. Reklaitis, "Dropwise Additive Manufacturing of Pharmaceutical Products for Melt-Based Dosage Forms," *Journal of Pharmaceutical Sciences,* p. 1641–1649, 2015.

[52] B. K. Lee, Y. Yun Hee, J. S. Choi, Y. C. Choi, J. D. Kim and Y. W. Cho, "Fabrication of drug-loaded polymer microparticles with arbitrary geometries using a piezoelectric inkjet printing system," *International Journal of Pharmaceutics,* 2012.

[53] M. Palo, K. Kogermann, L. I., A. Meos, M. Preis, J. Heinämäki and N. Sandler, "Development of Oromucosal Dosage Forms by Combining Electrospinning and Inkjet Printing," *Molecular Pharmaceutics,* vol. 14, no. 3, p. 808–820, 2017.

[54] D. Raijada, N. Genina, D. Fors, E. Wisaeus, J. Peltonen, J. Rantanen and N. Sandler, "A step toward development of printable dosage forms for poorly soluble drugs," *Journal of Pharmaceutical Sciences,* vol. 102, no. 10, p. 3694–3704, 2013.

[55] P. A. Melendez, K. M. Kane, C. S. Ashvar, M. Albrecht and P. A. Smith, "Thermal inkjet application in the preparation of oral dosage forms: dispensing of prednisolone solutions and polymorphic characterization by solid-state spectroscopic techniques," *Journal of Pharmaceutical Sciences,* vol. 97, no. 7, pp. 2619-2636, 2008.

[56] L.-D. Iftimi, M. Edinger, D. Bar-Shalom, J. Rantanen and N. Genina, "Edible solid foams as porous substrates for inkjet-printable pharmaceuticals," *European Journal of Pharmaceutics and Biopharmaceutics,* vol. 136, pp. 38-47, 2019.

[57] N. Genina, E. Janßen, A. Breitenbach, J. Breitkreutz and N. Sandler, "Evaluation of different substrates for inkjet printing of rasagiline mesylate," *European Journal of Pharmaceutics and Biopharmaceutics,* vol. 85, no. 3, pp. 1075-1083, 2013.

[58] A. B. M. Buanz, M. H. Saunders, A. W. Basit and S. Gaisford, "Preparation of personalized-dose salbutamol sulphate oral films with thermal ink-jet printing.," *Pharmaceutical Research,* vol. 28, no. 10, p. 2386–2392, 2011.

[59] C. Planchette, H. Pichler, M. Wimmer-Teubenbacher, M. Gruber, H. Gruber-Woelfler, S. Mohr, C. Tetyczka, W.-K. Hsiao, A. Paudel, E. Roblegg and J. Khinast, "Printing medicines as orodispersible dosage forms: Effect of substrate on the printed micro-structure," *International Journal of Pharmaceutics,* vol. 509, no. 1-2, pp. 518-527, 2017.

[60] M. Wimmer-Teubenbacher, C. Planchette, H. Pichler, D. Markl, W. K. Hsiao, A. Paudel and S. Stegemann, "Pharmaceutical-grade oral films as substrates for printed medicine," *International Journal of Pharmaceutics,* vol. 547, no. 1-2, pp. 169-180, 2018.

[61] H. K. Cader, G. A. Rance, M. R. Alexander, A. D. Gonçalves, C. J. Roberts, C. J. Tuck and R. D. Wildman, "Water-based 3D inkjet printing of an oral pharmaceutical dosage form," *International Journal of Pharmaceutics,* vol. 564, pp. 359-368, 2019.

[62] M. Alomari, P. R. Vuddanda, S. J. Trenfield, C. C. Dodoo, S. Velaga, A. W. Basit and S. Gaisford, "Printing T3 and T4 oral drug combinations as a novel strategy for hypothyroidism," *International Journal of Pharmaceutics,* vol. 549, no. 1-2, pp. 363-369, 2018.

[63] H. Öblom, E. Sjöholm, M. Rautamo and N. Sandler, "Towards Printed Pediatric Medicines in Hospital Pharmacies: Comparison of 2D and 3D-Printed Orodispersible Warfarin Films with Conventional Oral Powders in Unit Dose Sachets," *Pharmaceutics,* vol. 11, no. 7, p. 334, 2019.

[64] P. R. Vuddanda, M. Alomari, C. C. Dodoo, S. J. Trenfield, S. Velaga, A. W. Basit and S. Gaisford, "Personalisation of warfarin therapy using thermal ink-jet printing," *European Journal of Pharmaceutical Sciences,* vol. 117, pp. 80-87, 2018.

[65] N. Genina, D. Fors, M. Palo, J. Peltonen and N. Sandler, "Behavior of printable formulations of loperamide and caffeine on different substrates-Effect of print density in inkjet printing," *International Journal of Pharmaceutics,* vol. 453, no. 2, p. 488–497, 2013.

[66] G. Sharma, W. Mueannoom, A. B. Buanz, K. M. Taylor and S. Gaisford, "In vitro characterisation of terbutaline sulphate particles prepared by thermal ink-jet spray freeze drying," *International Journal of Pharmaceutics,* vol. 447, no. 1-2, pp. 165-170, 2013.

[67] P. J. Tarcha, D. Verlee, H. W. Hui, J. Setesak, B. Antohe, D. Radulescu and D. Wallace, "The application of ink-jet technology for the coating and loading of drug-eluting stents," *Annals of Biomedical Engineering,* vol. 35, no. 10, p. 1791–1799, 2007.

[68] L. Hirshfield, A. Giridhar, L. S. Taylor, M. Harris and G. Reklaitis, "Dropwise Additive Manufacturing of Pharmaceutical Products for Solvent-Based Dosage Forms," *Journal of Pharmaceutical Sciences,* vol. 103, no. 2, pp. 496-506, 2014.

[69] A. B. M. Buanz, M. H. Saunders, A. W. Basit and S. Gaisford, "Rapid preparation of pharmaceutical co-crystals with thermal ink-jet printing," *CrystEngComm,* vol. 15, no. 6, pp. 1031-1035, 2013.

[70] N. Scoutaris, A. L. Hook, P. R. Gellert, C. J. Roberts, M. R. Alexander and D. J. Scurr, "ToF-SIMS analysis of chemical heterogenities in inkjet micro-array printed drug/polymer formulations," *Journal of Materials Science: Materials in Medicine,* vol. 23, no. 2, pp. 385-391, 2012.

[71] P.-G. de Gennes, F. Brochard-Wyart and D. Quéré, Capillarity and Wetting Phenomena, Berlin: Springer-Verlag, 2004.

[72] N. Reis and B. Derby, "Ink Jet Deposition of Ceramic Suspensions: Modeling and Experiments of Droplet Formation," *MRS Online Proceedings Library,* vol. 624, no. 117, p. 65–70, 2000.

[73] N. Reisa, C. Ainsley and B. Derby, "Ink-jet delivery of particle suspensions by piezoelectric droplet ejectors," *Journal of Applied Physics,* vol. 97, no. 094903, 2005.

[74] T. Young, "An essay on cohesion of fluids," *Philosophical Transactions of the Royal Soiciety of London,* vol. 95, pp. 65-87, 1805.

[75] F. M. Fowkes, "Attractive Forces at Interfaces," *Industrial & Engineering Chemistry,* vol. 56, no. 12, pp. 40-52, 1964.

[76] D. K. Owens and R. C. Wendt, "Estimation of the surface free energy of polymers," *Journal of Applied Polymer Science,* vol. 13, no. 8, pp. 1741-1747, 1969.

[77] G. I. Loeb and M. Schrader, Modern Approaches to Wettability, New York: Springer US, 1992.

[78] A. M. Amado, M. M. Nolasco and P. J. A. Ribeiro-Claro, "Probing Pseudopolymorphic Transitions in Pharmaceutical Solids using Raman Spectroscopy: Hydration and Dehydration of Theophylline," *Journal of Pharmaceutical Sciences,* vol. 96, no. 5, pp. 1366-1379, 2007.

[79] A. V. Trask, W. D. S. Motherwell and W. Jonesa, "Physical stability enhancement of theophylline via cocrystallization," *International Journal of Pharmaceutics,* vol. 320, no. 1-2, pp. 114-123, 2006.

[80] "KRÜSS Advancing your Surface Science," KRÜSS GmbH, 2021. [Online]. Available: www.kruss-scientific.com. [Accessed 20 January 2021].

[81] H. Vakili, H. Wickström, D. Desai, M. Preis and N. Sandler, "Application of a handheld NIR spectrometer in prediction of drug content in inkjet printed orodispersible formulations containing prednisolone and levothyroxine," *International Journal of Pharmaceutics,* vol. 524, no. 1-2, pp. 414-423, 2017.

[82] N. C. f. B. Information, "PubChem Compound Summary for CID 2153, Theophylline," 2021. [Online]. Available: https://pubchem.ncbi.nlm.nih.gov/compound/Theophylline.. [Accessed 13 April 2021].

[83] H. Vakili, R. Kolakovic, N. Genina, M. Marmion and H. Salo, "Hyperspectral imaging in quality control of inkjet printed personalised dosage forms," *International Journal of Pharmaceutics,* vol. 483, no. 1-2, pp. 244-249, 2015.

[84] X. Zhang and O. A. Basaran, "Dynamic Surface Tension Effects in Impact of a Drop with a Solid Surface," *Journal of Colloid and Interface Science,* vol. 187, no. 1, pp. 166-178, 1997.

[85] J. L. Cohen, "Theophylline," *Analytical Profiles of Drug Substances,* vol. 4, no. 1975, pp. 466-493, 1975.

APPENDIX

IR spectra of paper samples printed with method 1

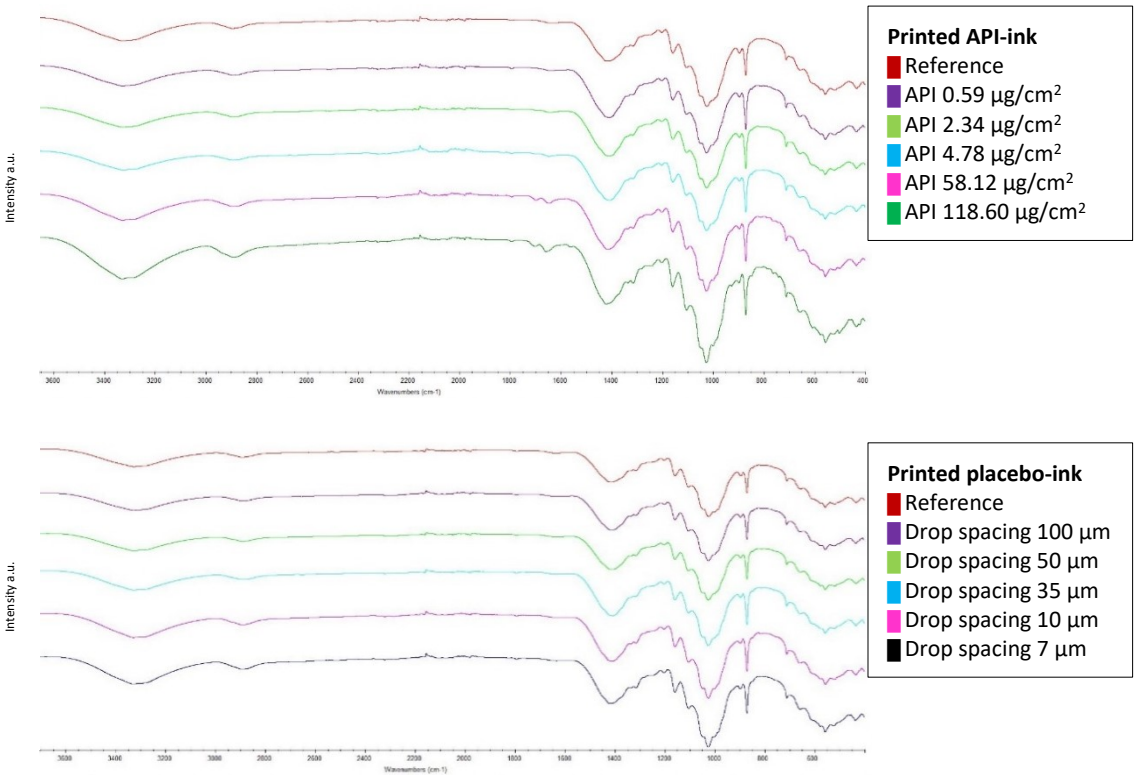

Figure 22. Transmittance IR spectra of paper samples of theophylline printed in five different concentrations (above) and the corresponding concentrations printed with the placebo ink (below). The concentrations were adjusted by changing the drop spacing (method 1). Reference spectrum of the plain substrate was also measured.

Microscope pictures and IR spectra of plexi samples printed with method 1

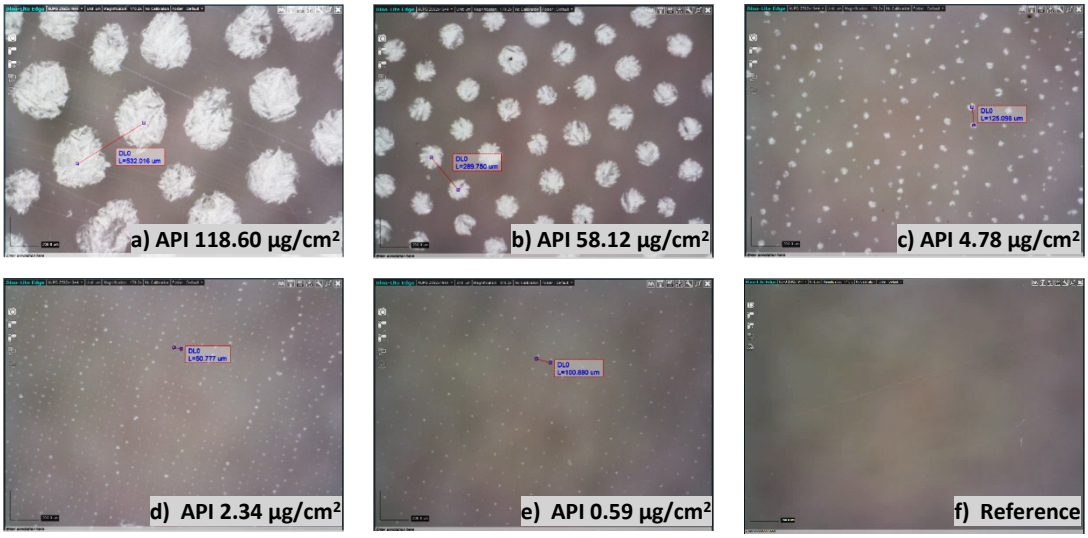

Figure 23. Theophylline printed on plexi in five different concentrations. The concentrations were adjusted by changing the drop spacing (method 1). The pictures were taken with the same zoom-setting and the spacing between the printed, dried dots was measured with the software.

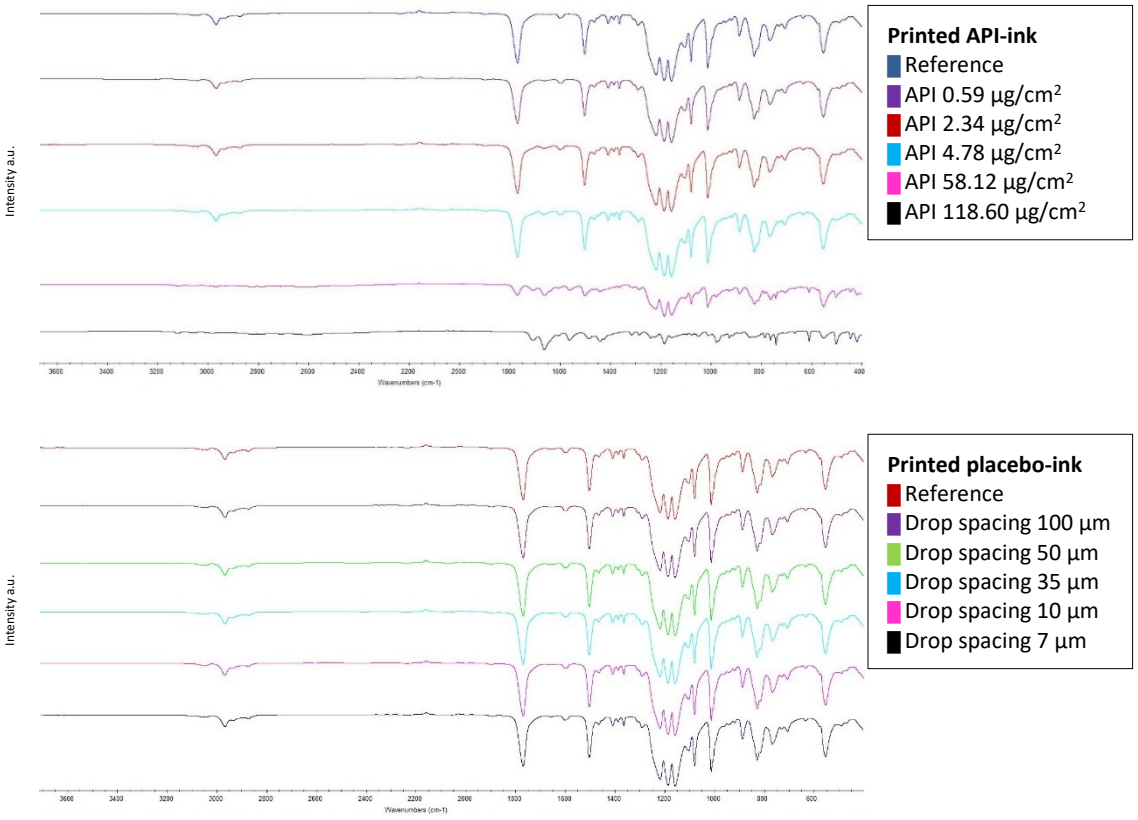

Figure 24. Transmittance IR spectra of plexi samples of theophylline printed in five different concentrations (above) and the corresponding concentrations printed with the placebo ink (below). The concentrations were adjusted by changing the drop spacing (method 1). Reference spectrum of the plain substrate was also measured.

Microscope pictures and IR spectra of rubber samples printed with method 1

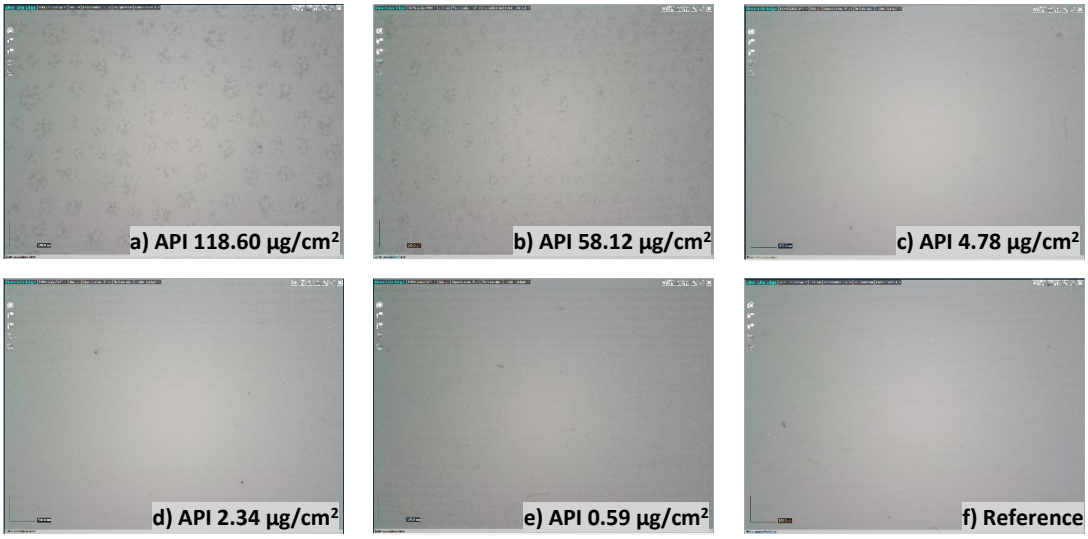

Figure 25. Theophylline printed on rubber in five different concentrations. The concentrations were adjusted by changing the drop spacing (method 1). The pictures were taken with the same zoom-setting.

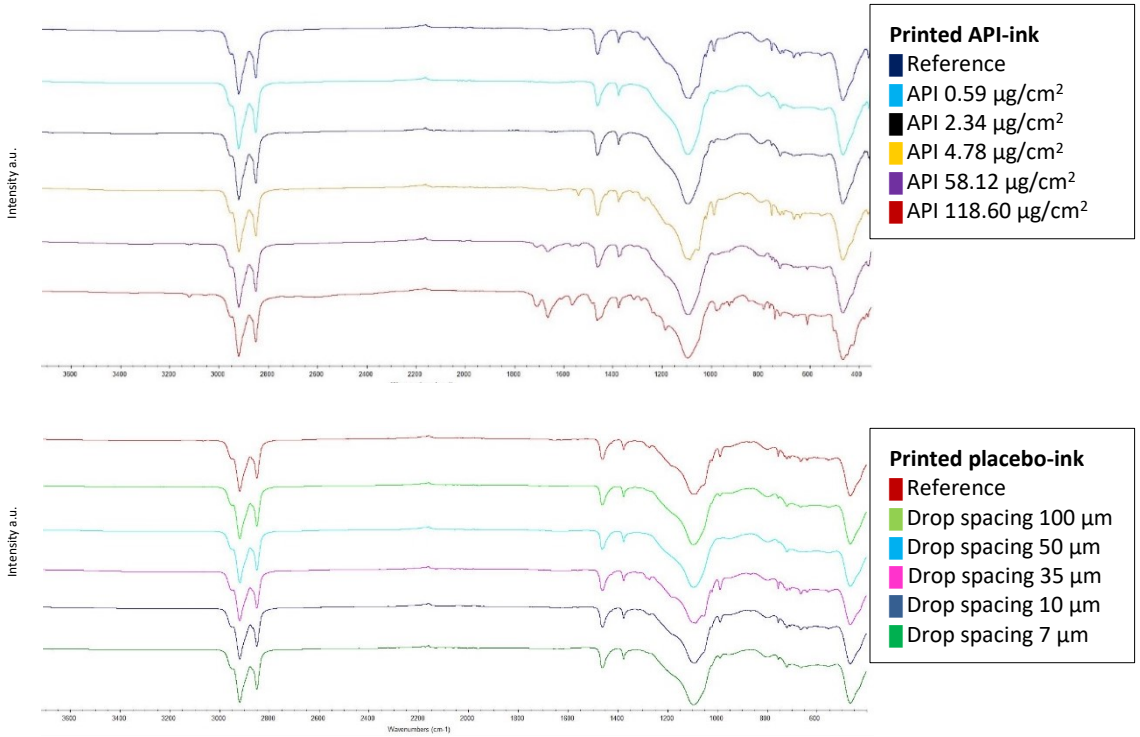

Figure 26. Transmittance IR spectra of rubber samples of theophylline printed in five different concentrations (above) and the corresponding concentrations printed with the placebo ink (below). The concentrations were adjusted by changing the drop spacing (method 1). Reference spectrum of the plain substrate was also measured.

Microscope pictures and IR spectra of enamel samples printed with method 1

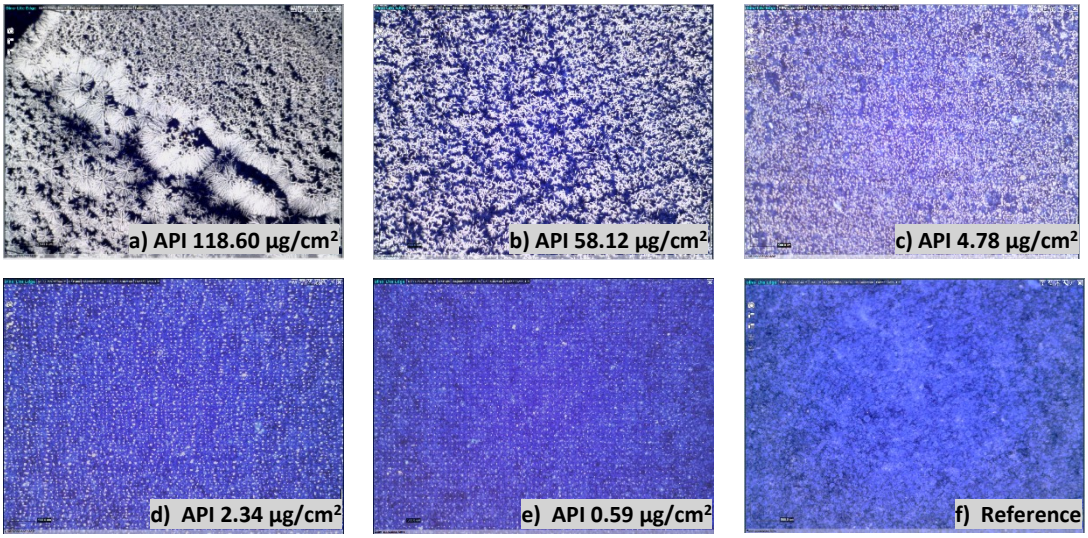

Figure 27. Theophylline printed on enamel in five different concentrations. The concentrations were adjusted by changing the drop spacing (method 1). The pictures were taken with the same zoom-setting.

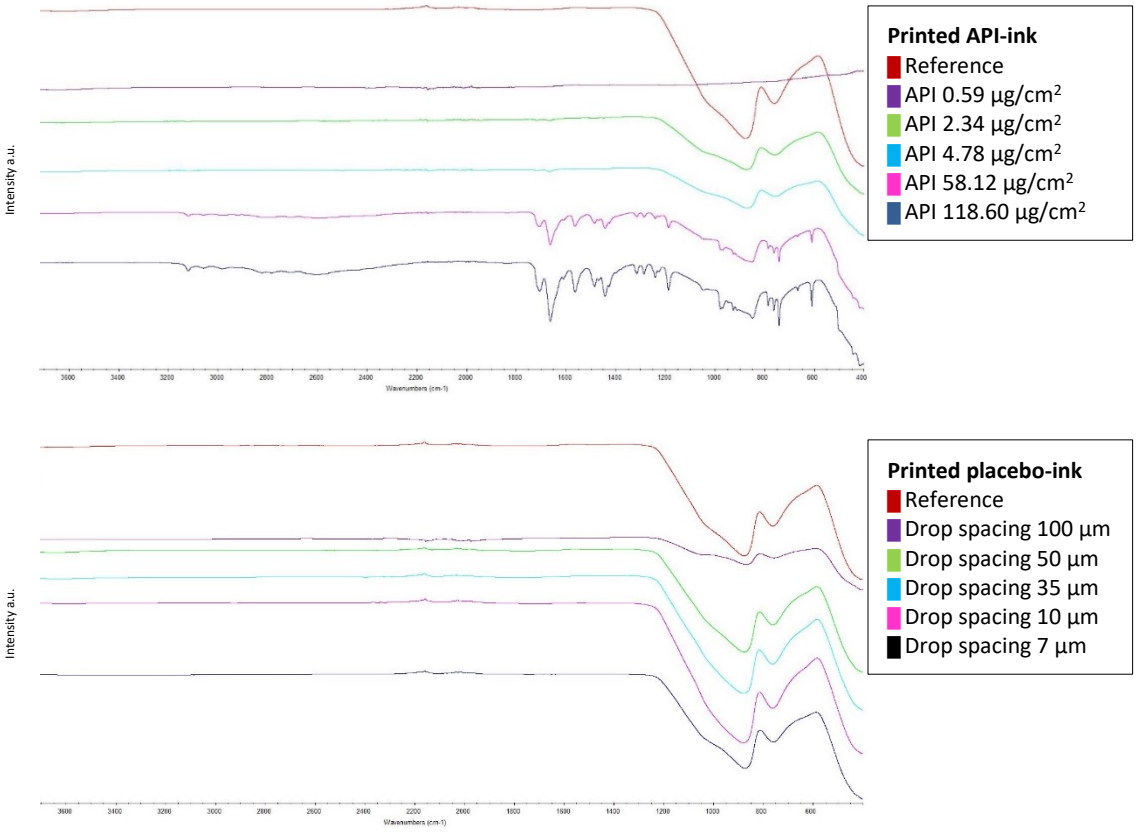

Figure 28. Transmittance IR spectra of enamel samples of theophylline printed in five different concentrations (above) and the corresponding concentrations printed with the placebo ink (below). The concentrations were adjusted by changing the drop spacing (method 1). Reference spectrum of the plain substrate was also measured. Due to an uneven sample plate, the FTIR-ATR measurements for printed API concentration of 0.59 µg/cm² failed.

Microscope pictures and IR spectra of epoxy samples printed with method 1

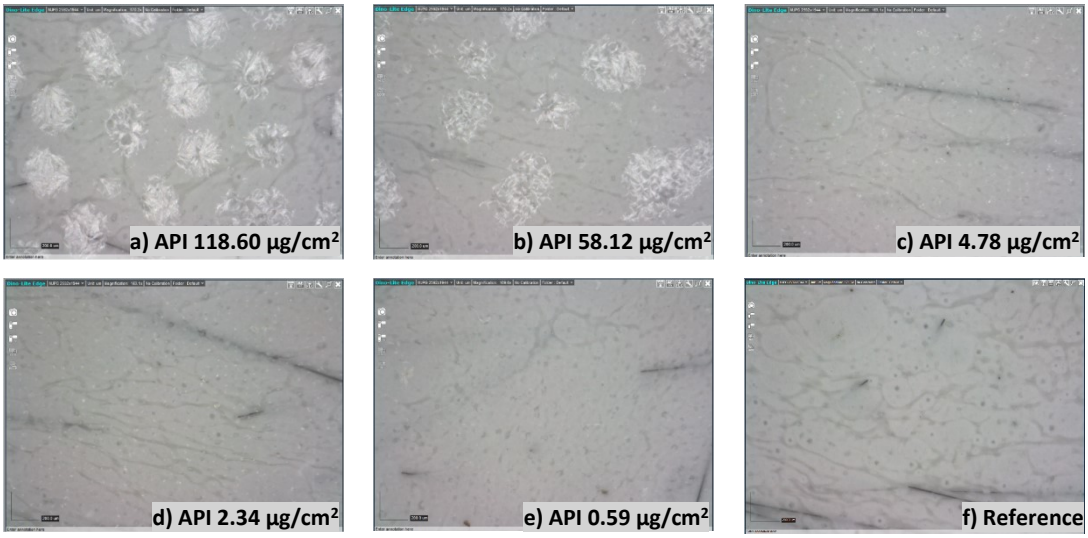

Figure 29. Theophylline printed on epoxy in five different concentrations. The concentrations were adjusted by changing the drop spacing (method 1). The pictures were taken with the same zoom-setting.

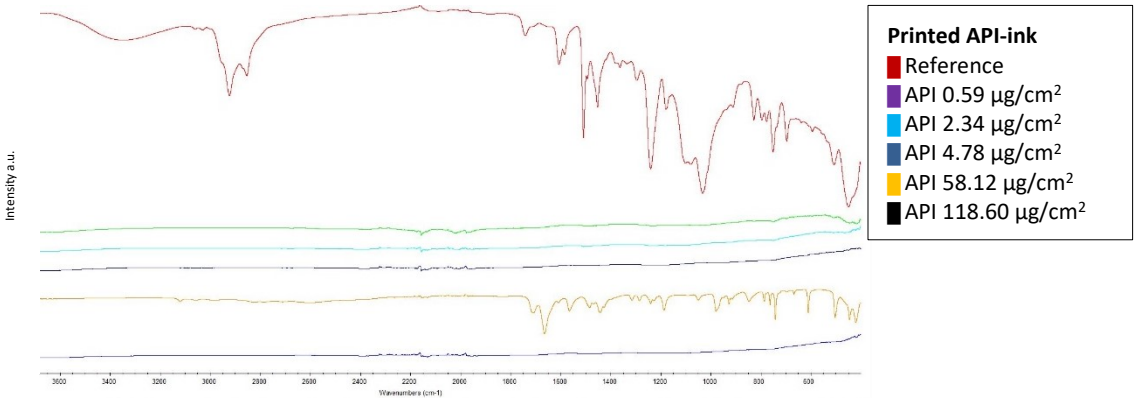

Figure 30. Transmittance IR spectra of epoxy samples of theophylline printed in five different concentrations. The concentrations were adjusted by changing the drop spacing (method 1). Reference spectrum of the plain substrate was also measured. Due to an uneven sample plate, most of the FTIR-ATR measurements failed.

Microscope pictures and IR spectra of steel samples printed with method 1

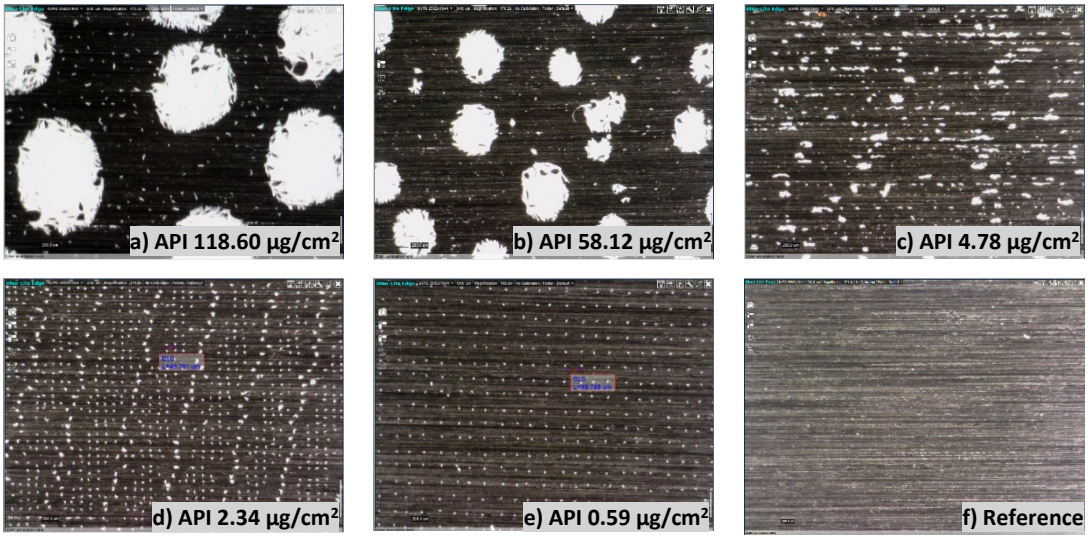

Figure 31. Theophylline printed on steel in five different concentrations. The concentrations were adjusted by changing the drop spacing (method 1). The pictures were taken with the same zoom-setting.

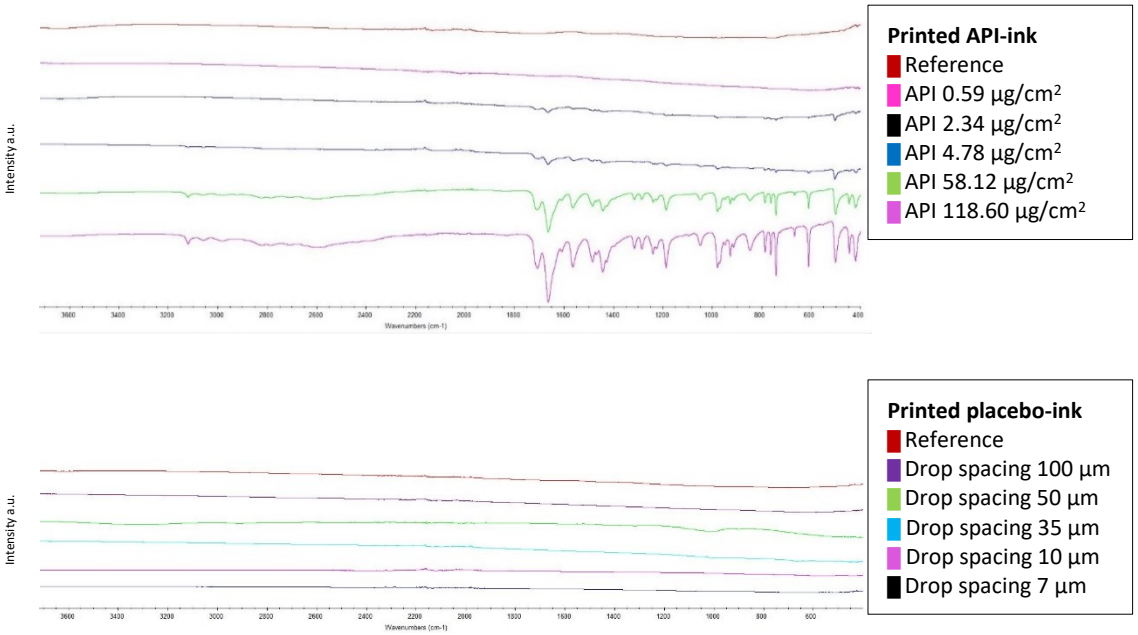

Figure 32. Transmittance IR spectra of steel samples of theophylline printed in five different concentrations (above) and the corresponding concentrations printed with the placebo ink (below). The concentrations were adjusted by changing the drop spacing (method 1). Reference spectrum of the plain substrate was also measured.

Microscope pictures and IR spectra of steel samples printed with method 2

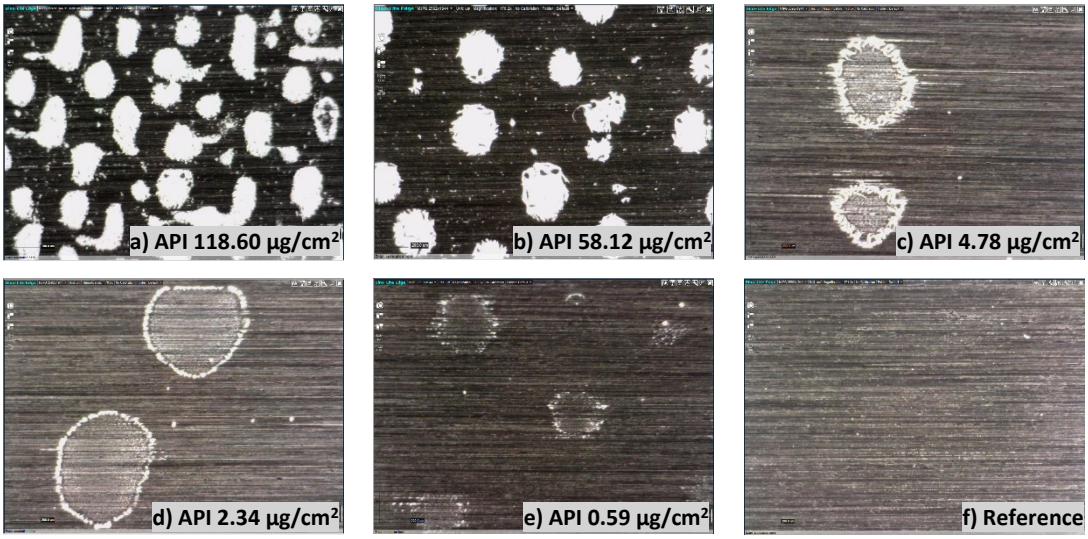

Figure 33. Theophylline printed on steel in five different concentrations. The printed concentrations were adjusted by the API concentration in the ink (method 2). The pictures were taken with the same zoom-setting.

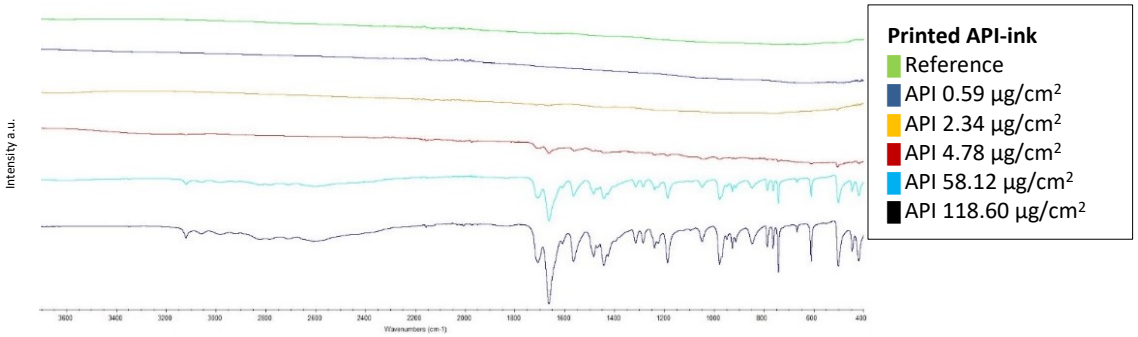

Figure 34. Transmittance IR spectra of steel samples of theophylline printed in five different concentrations. The printed concentrations were adjusted by the API concentration in the ink (method 2). Reference spectrum of the plain substrate was also measured.

Microscope pictures and IR spectra of aluminum samples printed with method 1

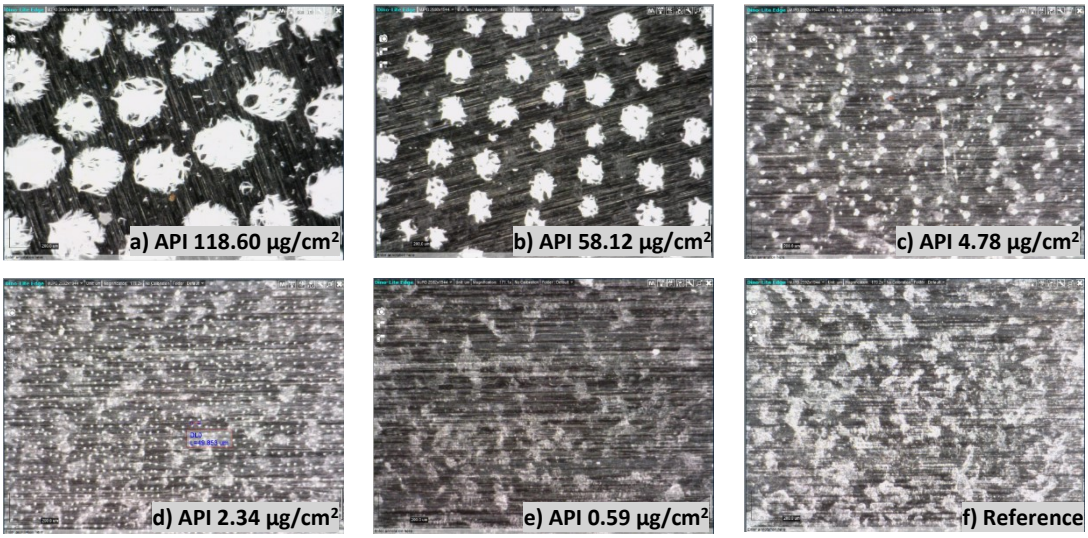

Figure 35. Theophylline printed on aluminum in five different concentrations. The concentrations were adjusted by changing the drop spacing (method 1). The pictures were taken with the same zoom-setting.

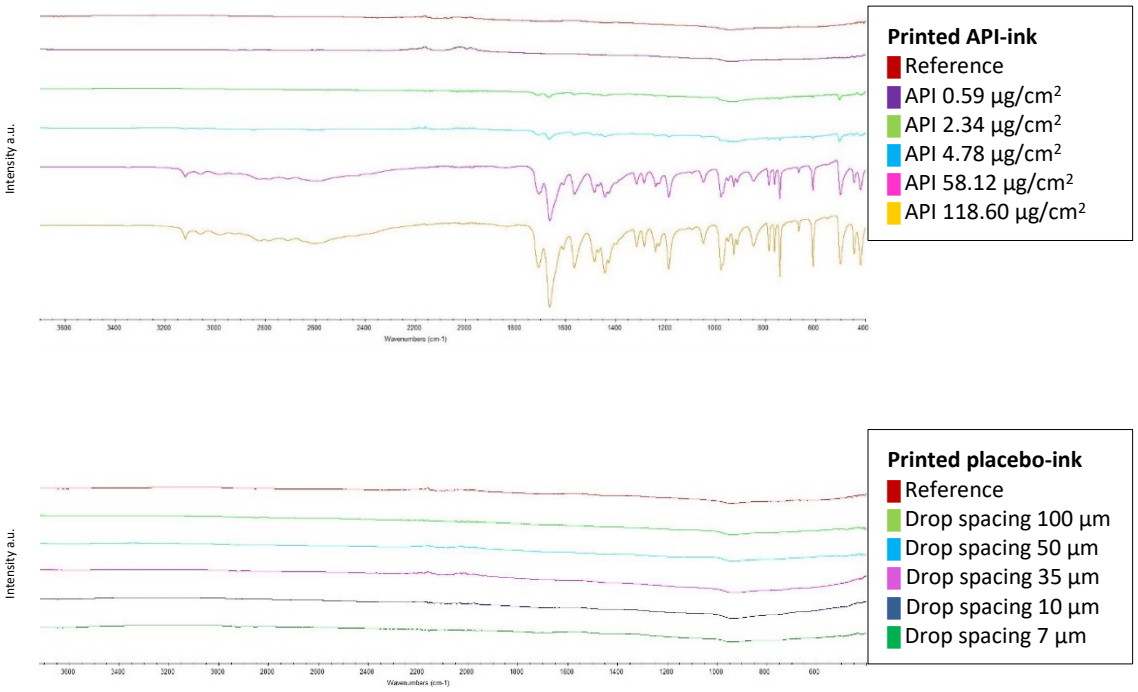

Figure 36. Transmittance IR spectra of aluminum samples of theophylline printed in five different concentrations (above) and the corresponding concentrations printed with the placebo ink (below). The concentrations were adjusted by changing the drop spacing (method 1). Reference spectrum of the plain substrate was also measured.

Microscope pictures and IR spectra of aluminum samples printed with method 2

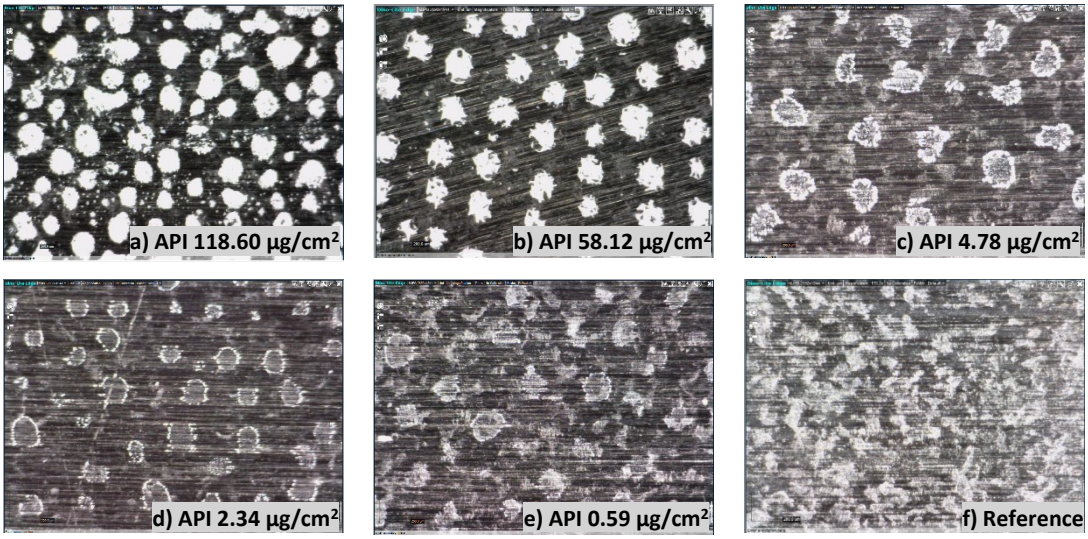

Figure 37. Theophylline printed on aluminum in five different concentrations. The printed concentrations were adjusted by the API concentration in the ink (method 2). The pictures were taken with the same zoom-setting.

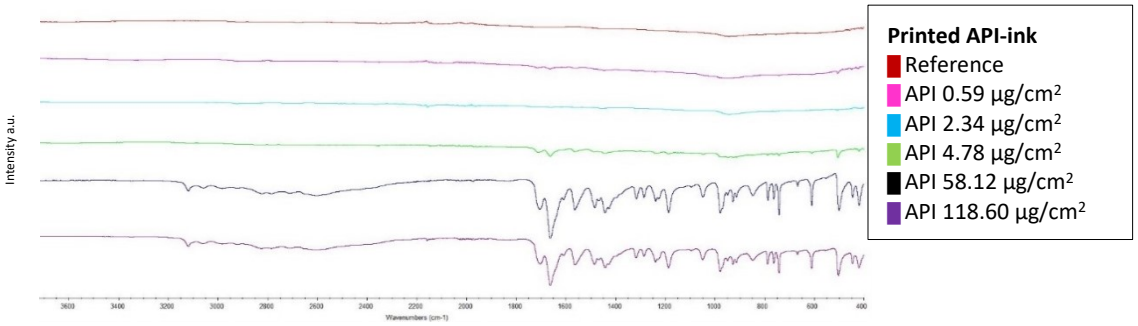

Figure 38. Transmittance IR spectra of theophylline printed on aluminum in five different concentrations. The printed concentrations were adjusted by the API concentration in the ink (method 2) and the samples were dried in vacuum overnight. Reference spectrum of the plain substrate was also measured.

Microscope pictures and IR spectra of glass samples printed with method 1

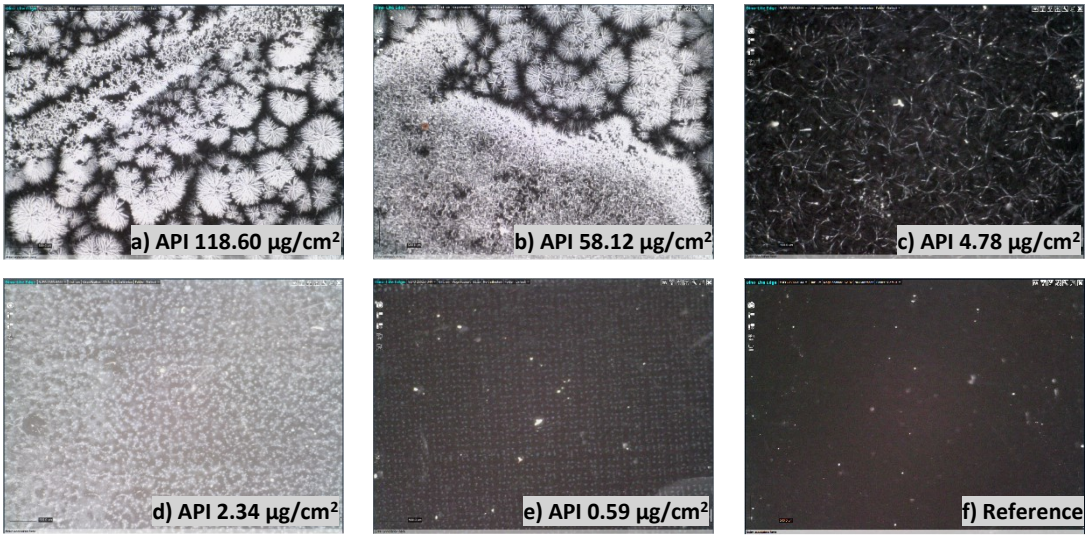

Figure 39. Theophylline printed on glass in five different concentrations. The concentrations were adjusted by changing the drop spacing (method 1). The pictures were taken with the same zoom-setting.

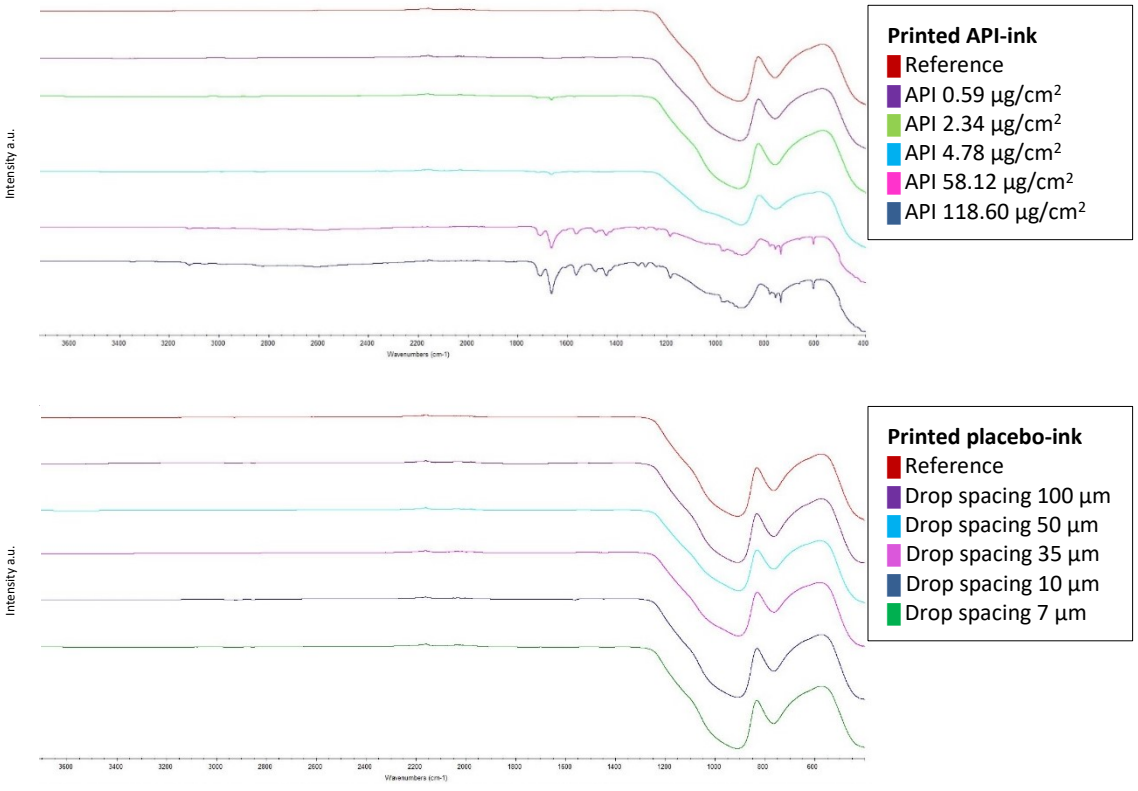

Figure 40. Transmittance IR spectra of glass samples of theophylline printed in five different concentrations (above) and the corresponding concentrations printed with the placebo ink (below). The concentrations were adjusted by changing the drop spacing (method 1). Reference spectrum of the plain substrate was also measured.

Microscope pictures and IR spectra of glass samples printed with method 2

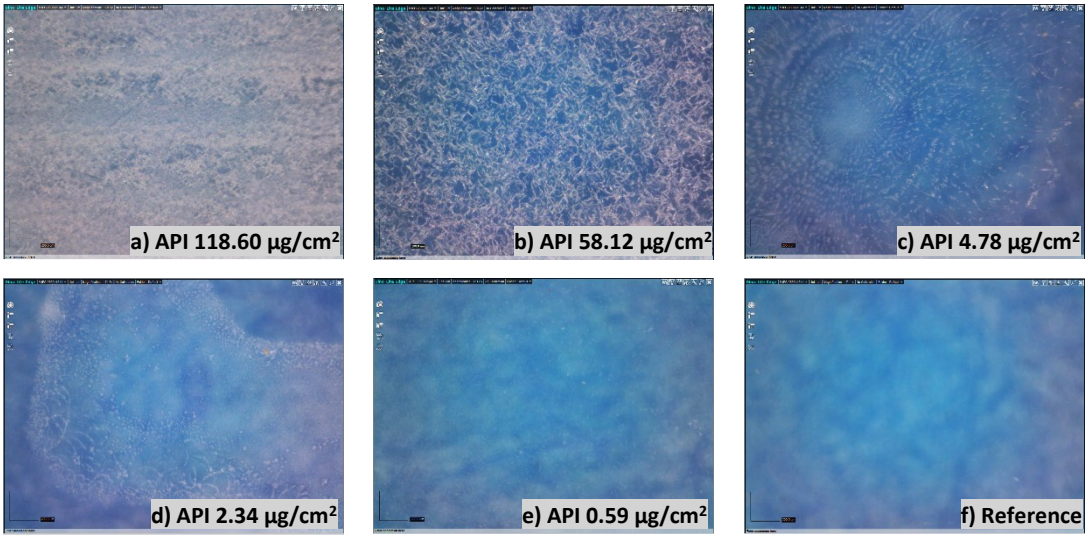

Figure 41. Theophylline printed on glass in five different concentrations. The printed concentrations were adjusted by the API concentration in the ink (method 2). The pictures were taken with the same zoom-setting.

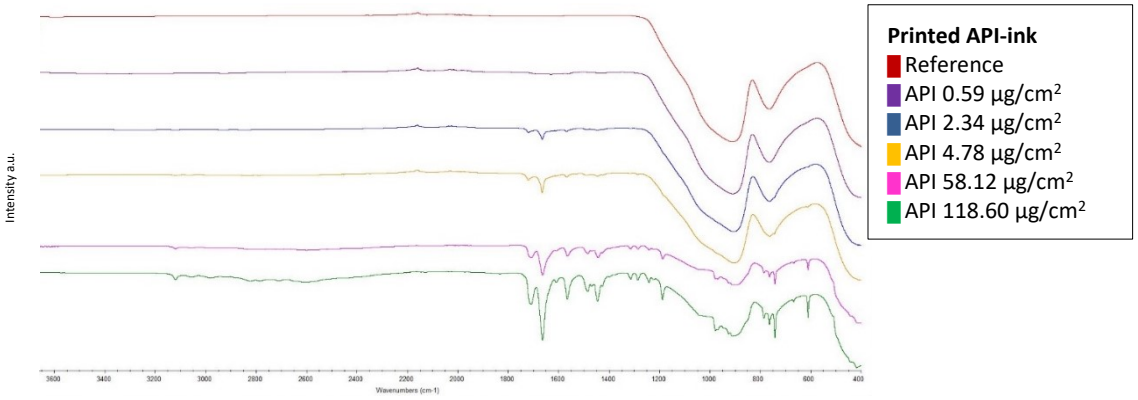

Figure 42. Transmittance IR spectra of theophylline printed on aluminum in five different concentrations. The printed concentrations were adjusted by the API concentration in the ink (method 2) and the samples were dried in vacuum overnight. Reference spectrum of the plain substrate was also measured.

Microscope pictures and IR spectra of glass samples printed with method 3

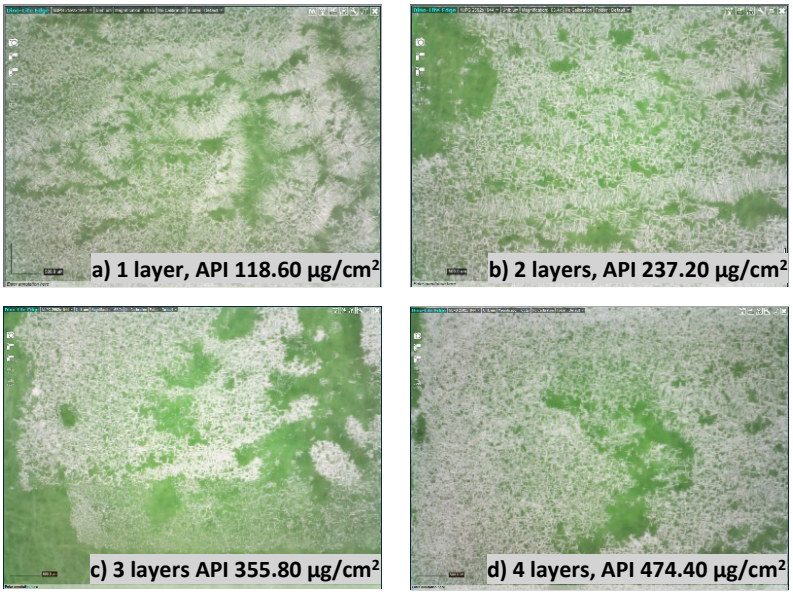

Figure 43. Theophylline printed on glass in four different concentrations. The printed API concentrations were adjusted by printing layers of ink on top of one another (method 3) with overnight vacuum dying in between printed layers. The pictures were taken with the same zoom-setting.

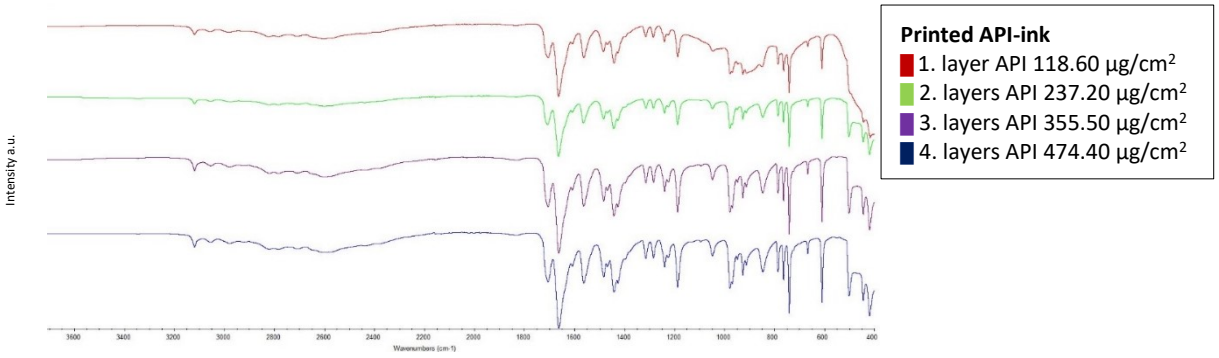

Figure 44. Transmittance IR spectra of theophylline printed on glass in four different concentrations. The printed API concentrations were adjusted by printing layers of ink on top of one another (method 3) with overnight vacuum dying in between printed layers.